

Synthesis and Characterization of Ruthenium Bis(β -diketonato) Pyridine-Imidazole Complexes for Hydrogen Atom Transfer

Adam Wu, Joshua Masland, Rodney D. Swartz,[†] Werner Kaminsky,[†] and James M. Mayer*

Department of Chemistry, University of Washington, Campus Box 351700, Seattle, Washington 98195-1700

Received August 7, 2007

Ruthenium bis(β -diketonato) complexes have been prepared at both the Ru^{II} and Ru^{III} oxidation levels and with protonated and deprotonated pyridine–imidazole ligands. Ru^{II}(acac)₂(py-imH) (**1**), [Ru^{III}(acac)₂(py-imH)]OTf (**2**), Ru^{III}(acac)₂(py-im) (**3**), Ru^{II}(hfac)₂(py-imH) (**4**), and [DBU–H][Ru^{II}(hfac)₂(py-im)] (**5**) have been fully characterized, including X-ray crystal structures (acac = 2,4-pentanedionato, hfac = 1,1,1,5,5,5-hexafluoro-2,4-pentanedionato, py-imH = 2-(2'-pyridyl)imidazole, DBU = 1,8-diazabicyclo[5.4.0]undec-7-ene). For the acac-imidazole complexes **1** and **2**, cyclic voltammetry in MeCN shows the Ru^{III/II} reduction potential ($E_{1/2}$) to be -0.64 V versus Cp₂Fe⁺⁰. $E_{1/2}$ for the deprotonated imidazolate complex **3** (-1.00 V) is 0.36 V more negative. The Ru^{II} bis-hfac analogues **4** and **5** show the same $\Delta E_{1/2} = 0.36$ V but are 0.93 V harder to oxidize than the acac derivatives (0.29 and -0.07 V). The difference in acidity between the acac and hfac derivatives is much smaller, with pK_a values of 22.1 and 19.3 in MeCN for **1** and **4**, respectively. From the $E_{1/2}$ and pK_a values, the bond dissociation free energies (BDFEs) of the N–H bonds in **1** and **4** are calculated to be 62.0 and 79.6 kcal mol⁻¹ in MeCN – a remarkable difference of 17.6 kcal mol⁻¹ for such structurally similar compounds. Consistent with these values, there is a facile net hydrogen atom transfer from **1** to TEMPO[•] (2,2,6,6-tetramethylpiperidine-1-oxyl radical) to give **3** and TEMPO–H. The ΔG° for this reaction is -4.5 kcal mol⁻¹. **4** is not oxidized by TEMPO[•] ($\Delta G^\circ = +13.1$ kcal mol⁻¹), but in the reverse direction TEMPO–H readily reduces in situ generated Ru^{III}(hfac)₂(py-im) (**6**). A Ru^{II}-imidazoline analogue of **1**, Ru^{II}(acac)₂(py-imnH) (**7**), reacts with 3 equiv of TEMPO[•] to give the imidazolate **3** and TEMPO–H, with dehydrogenation of the imidazoline ring.

Introduction

Proton-coupled electron transfer (PCET) is a fundamental process in chemistry and biology.^{1,2} Hydrogen atom transfer (HAT) reactions are one class of PCET processes, in which a hydrogen atom ($H^\bullet = H^+ + e^-$) concertedly transfers from one reagent to another in a single kinetic step. HAT reactions of transition-metal species are receiving much attention because of their role in metal-catalyzed oxidations, ranging from metal-oxide surfaces to various metalloenzymes.^{1–5} To

cite just one example, the peroxidation of polyunsaturated fatty acids is catalyzed by lipoxygenases using HAT from the substrate to the active site Fe^{III}OH center, forming the Fe^{II}OH₂ moiety and the substrate pentadienyl radical.⁴ As this example illustrates, many metal-mediated HAT reactions involve a redox change at the metal, coupled to a change in the protonation state of the ligand.^{1–3,5} These systems can be described by the square scheme in Scheme 1, with electron

* To whom correspondence should be addressed. E-mail: mayer@chem.washington.edu.

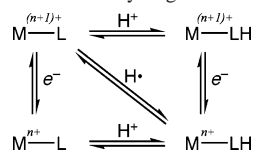
[†] UW Chemistry crystallographic facility.

(1) (a) Cukier, R. I.; Nocera, D. G. *Annu. Rev. Phys. Chem.* **1998**, *49*, 337. (b) Hodgkiss, J. M.; Rosenthal, J.; Nocera, D. G. In *Hydrogen-Transfer Reactions*; Hynes, J. T., Klinman, J. P., Limbach, H.-H., Schowen, R. L., Eds.; Wiley-VCH: Weinheim, Germany, 2007; Vol. 2, pp 503–562. (c) Stubbe, J.; Nocera, D. G.; Yee, C. S.; Chang, M. C. Y. *Chem. Rev.* **2003**, *103*, 2167. (d) Hammes-Schiffer, S. In *Hydrogen-Transfer Reactions*; Hynes, J. T., Klinman, J. P., Limbach, H.-H., Schowen, R. L., Eds.; Wiley-VCH: Weinheim, Germany, 2007; Vol. 2, pp 479–502. (e) Meyer, T. J.; Huynh, M. H. V. *Inorg. Chem.* **2003**, *42*, 8140.

(2) (a) Mayer, J. M. *Annu. Rev. Phys. Chem.* **2004**, *55*, 363. (b) Mayer, J. M.; Rhile, I. J. *Biochim. Biophys. Acta* **2004**, *1655*, 51. (c) Mayer, J. M.; Rhile, I. J.; Larsen, F. B.; Mader, E. A.; Markle, T. F.; DiPasquale, A. G. *Photosynth. Res.* **2006**, *87*, 3. (d) Mayer, J. M.; Mader, E. A.; Roth, J. P.; Bryant, J. R.; Matsuo, T.; Dehestani, A.; Bales, B. C.; Watson, E. J.; Osako, T.; Valliant-Saunders, K.; Lam, W.-H.; Hrovat, D. A.; Borden, W. T.; Davidson, E. R. *J. Mol. Catal. A: Chem.* **2006**, *251*, 24.

(3) Mayer, J. M. *Acc. Chem. Res.* **1998**, *31*, 441.

(4) (a) Knapp, M. J.; Meyer, M.; Klinman, J. P. In *Hydrogen-Transfer Reactions*; Hynes, J. T., Klinman, J. P., Limbach, H.-H., Schowen, R. L., Eds.; Wiley-VCH: Weinheim, Germany, 2007; Vol. 4, pp 1241–1284. (b) Knapp, M. J.; Rickert, K.; Klinman, J. P. *J. Am. Chem. Soc.* **2002**, *124*, 3865. (c) Glickman, M. H.; Klinman, J. P. *Biochemistry* **1996**, *35*, 12882.

Scheme 1. Square Scheme for Hydrogen Atom Transfer

transfer (ET) and proton transfer (PT) reactions as the edges and HAT as the diagonal.²

Our group has been building an understanding of metal-mediated HAT reactions by developing chemical systems in which both the thermodynamics and kinetics of HAT can be determined. Isolation of at least three corners of the square greatly facilitates these measurements. Among the systems we have studied, iron-tris(biimidazole) complexes have been particularly informative in part because the Fe^{II}-protonated, Fe^{III}-protonated, and Fe^{III}-deprotonated complexes are all readily isolated.⁶ We have examined in detail the thermochemistry of this system, including its large entropy for HAT reactions, oxidations of C–H and O–H bonds, rate constants for cross and self-exchange rates, and the agreement with the Marcus cross relation.^{6a,b,7}

A ruthenium system is of interest to test the generality of our HAT conclusions and to explore the analogies between HAT and ET. ET processes of ruthenium complexes have been studied in great detail,⁸ in part because the substitution-inert nature of low-spin Ru^{II} complexes provides valuable stability and synthetic flexibility. The groups of Hammarström,⁹ Kramer,¹⁰ Nocera,^{11a,b} and Meyer^{11c} have each developed elegant ruthenium–polypyridyl systems for PCET studies. These systems involve stable Ru^{II} complexes and the photolytic generation of the corresponding Ru^{III} complexes. Whereas photolytic initiation of reactions is of great value for certain measurements, these systems are also limited by difficulties in isolating the Ru^{III} species because of their high reduction potentials.

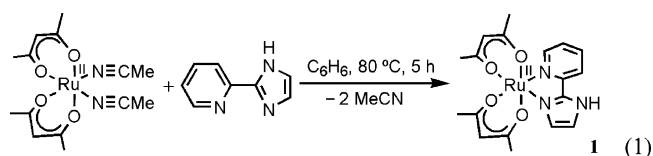
Our design criteria for a ruthenium PCET system were (i) suitable one-electron reduction potentials so that both Ru^{II}

and Ru^{III} species could be isolated and (ii) the ability to prepare protonated and mono-deprotonated derivatives. After some initial efforts, which are described below, we have developed a system with acac (2,4-pentanedionato) and 2-(2'-pyridyl)imidazole (py-imH) ligands, such as Ru^{II}(acac)₂(py-imH) (**1**), in which three corners of the square have been isolated. Py-imH is a well-known chelating ligand with a single ionizable proton,^{12,13} and stable Ru^{II}/Ru^{III} pairs with two acac ligands have been reported, including *cis*-Ru^{II}(acac)₂(MeCN)₂/*cis*-[Ru^{III}(acac)₂(MeCN)₂]OTf^{14,15} and Ru^{II}(acac)₂(bpy)/[Ru^{III}(acac)₂(bpy)]OTf¹⁶ (bpy = 2,2'-bipyridine; OTf⁻ = triflate, CF₃SO₃⁻). The related pyridine–imidazole complexes with hexafluoro-acac (1,1,1,5,5,5-hexafluoro-2,4-pentanedionato, hfac) ligand have also been prepared in this work. Described here are the syntheses and characterization of the compounds that comprise new ruthenium PCET systems, together with thermochemical measurements and preliminary studies of their HAT reactions.

Results

Syntheses. Attempts to develop a ruthenium system analogous to the iron-tris(biimidazole) complexes started with the known tris(biimidazole) complex [Ru^{II}(H₂bibzim)₃](ClO₄)₂ (H₂bibzim = 2,2'-bibenzimidazole).¹⁷ Unlike the iron system, [Ru^{II}(H₂bibzim)₃](ClO₄)₂ appears to doubly deprotonate upon titration with base, which made the study of HAT reactions problematic.¹⁸ To circumvent this issue, [Ru^{II}(bpy)₂(2-(2'-pyridyl)benzimidazole)](ClO₄)₂, which contains only one protonation site, was synthesized.¹³ However, this complex has a high Ru^{III/II} reduction potential ($E_{1/2} = 0.86$ V vs Cp₂Fe⁺⁰ in MeCN¹⁹), and in our hands isolation of the Ru^{III} derivative was not possible.¹⁸

Following these initial efforts, we turned our attention to Ru(acac)₂ complexes of 2-(2'-pyridyl)imidazole (py-imH) and 2-(2'-pyridyl)imidazole (py-imnH). The latter complexes have more complex HAT chemistry, as described below, so we start here with the aromatic py-imH compounds. Treatment of *cis*-Ru^{II}(acac)₂(MeCN)₂¹⁴ with 1.2 equiv of py-imH¹² in C₆H₆ for 5 h at 80 °C under N₂ forms Ru^{II}(acac)₂(py-imH) (**1**) as a light-brown precipitate, which was isolated by filtration in 78% yield (eq 1). **1** is very air-



- (5) There are also many examples of HAT-involving metal hydride complexes, for instance: (a) Song, J.-S.; Bullock, R. M.; Creutz, C. *J. Am. Chem. Soc.* **1991**, *113*, 9862. (b) Edidin, R. T.; Sullivan, J. M.; Norton, J. R. *J. Am. Chem. Soc.* **1987**, *109*, 3945.
- (6) (a) Roth, J. P.; Lovell, S.; Mayer, J. M. *J. Am. Chem. Soc.* **2000**, *122*, 5486. (b) Roth, J. P.; Mayer, J. M. *Inorg. Chem.* **1999**, *38*, 2760. (c) Burnett, M. G.; McKee, V.; Nelson, S. M. *J. Chem. Soc., Dalton Trans.* **1981**, 1492. (d) Wang, J. C.; Bauman, J. E., Jr. *Inorg. Chem.* **1965**, *4*, 1613.
- (7) (a) Roth, J. P.; Yoder, J. C.; Won, T.-J.; Mayer, J. M. *Science* **2001**, *294*, 2524. (b) Mader, E. A.; Davidson, E. R.; Mayer, J. M. *J. Am. Chem. Soc.* **2007**, *129*, 5153. (c) Mader, E. A.; Larsen, A. S.; Mayer, J. M. *J. Am. Chem. Soc.* **2004**, *126*, 8066. (d) Yoder, J. C.; Roth, J. P.; Gussenhoven, E. M.; Larsen, A. S.; Mayer, J. M. *J. Am. Chem. Soc.* **2003**, *125*, 2629.
- (8) (a) Wherland, S. *Coord. Chem. Rev.* **1993**, *123*, 169. (b) Meyer, T. J.; Taube, H. In *Comprehensive Coordination Chemistry*; Wilkinson, G. Ed.; Pergamon: New York, 1987; Vol. 1, pp 331–384.
- (9) (a) Lomoth, R.; Magnuson, A.; Sjödin, M.; Huang, P.; Styring, S.; Hammarström, L. *Photosynth. Res.* **2006**, *87*, 25. (b) Sjödin, M.; Styring, S.; Wolpher, H.; Xu, Y.; Sun, L.; Hammarström, L. *J. Am. Chem. Soc.* **2005**, *127*, 3855.
- (10) Cape, J. L.; Bowman, M. K.; Kramer, D. M. *J. Am. Chem. Soc.* **2005**, *127*, 4208.
- (11) (a) Roberts, J. A.; Kirby, J. P.; Nocera, D. G. *J. Am. Chem. Soc.* **1995**, *117*, 8051. (b) Kirby, J. P.; Roberts, J. A.; Nocera, D. G. *J. Am. Chem. Soc.* **1997**, *119*, 9230. (c) Facenko, C. J.; Meyer, T. J.; Thorp, H. H. *J. Am. Chem. Soc.* **2006**, *128*, 11020.

- (12) Hughey, J. L.; IV; Knapp, S.; Schugar, H. *Synthesis* **1980**, *6*, 489.
- (13) (a) Haga, M. *Inorg. Chim. Acta* **1983**, *75*, 29. (b) Haga, M.; Tsunemitsu, A. *Inorg. Chim. Acta* **1989**, *164*, 137.
- (14) Baird, I. R.; Cameron, B. R.; Skerlj, R. T. *Inorg. Chim. Acta* **2003**, *353*, 107.
- (15) Baird, I. R.; Rettig, S. J.; James, B. R.; Skov, K. A. *Can. J. Chem.* **1999**, *77*, 1821.
- (16) El-Hendawy, A. M.; Alqaradawi, S. Y.; Al-Madfa, H. A. *Transition Met. Chem.* **2000**, *25*, 572.
- (17) Haga, M. *Inorg. Chim. Acta* **1983**, *77*, L39.
- (18) Carter, E.; Kanzelberger, M. A. Unpublished data, 2003.
- (19) Potential converted from Ru^{III/II} $E_{1/2} = 1.17$ V versus SCE using $E_{1/2}(\text{Cp}_2\text{Fe}^{+0}) = 0.31$ V versus SCE.^{13a}

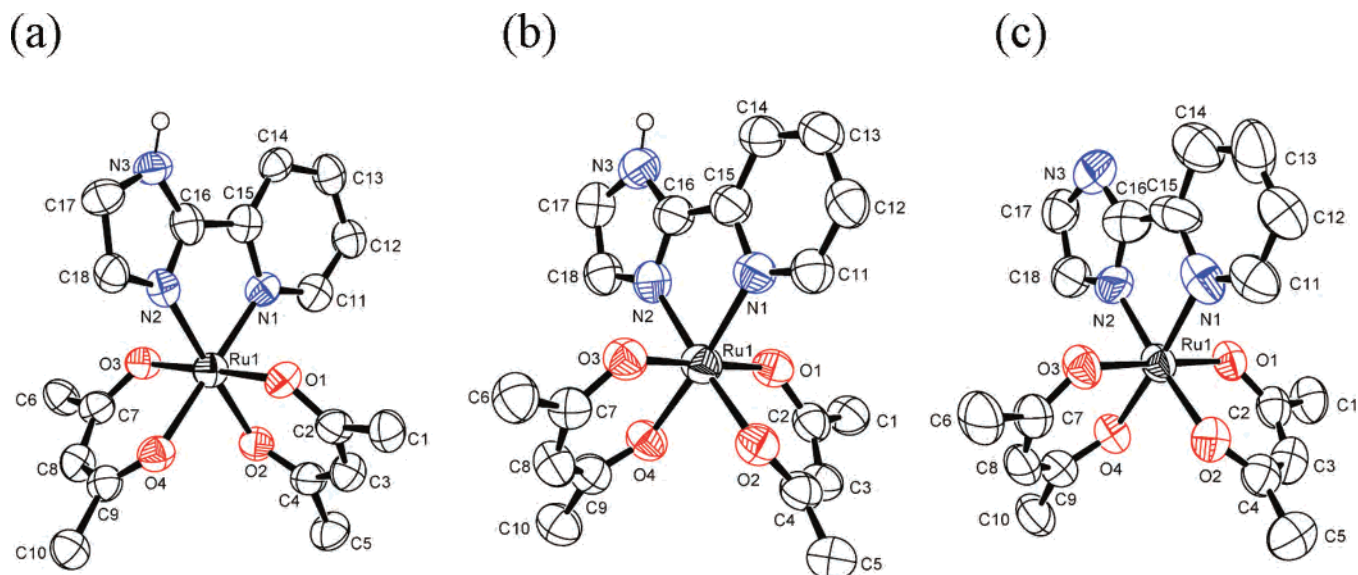
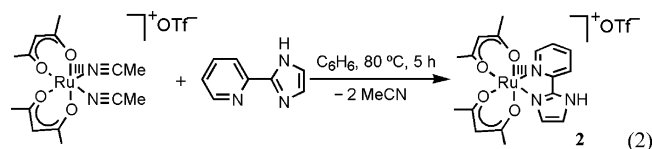
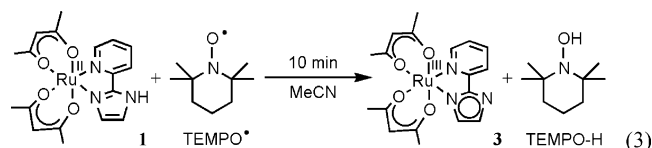


Figure 1. ORTEP drawings of (a) $\text{Ru}^{\text{II}}(\text{acac})_2(\text{py-imH})$ (**1**), (b) $[\text{Ru}^{\text{III}}(\text{acac})_2(\text{py-imH})]^+$ (**2**), and (c) $\text{Ru}^{\text{III}}(\text{acac})_2(\text{py-im})$ (**3**). Hydrogen atoms are omitted for clarity except for the N–H atom.

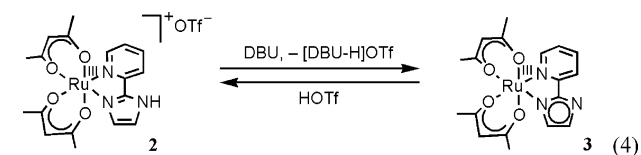
sensitive in solution, but less so in the solid state. The Ru^{II} analogue $[\text{Ru}^{\text{III}}(\text{acac})_2(\text{py-imH})]\text{OTf}$ (**2**) was prepared similarly by reacting *cis*- $[\text{Ru}^{\text{III}}(\text{acac})_2(\text{MeCN})_2]\text{OTf}^{15}$ with 1.2 equiv of py-imH to give a brick-red solid in 74% yield (eq 2). The deprotonated Ru^{III} derivative $\text{Ru}^{\text{III}}(\text{acac})_2(\text{py-im})$



(**3**) is most easily prepared by the removal of a hydrogen atom from **1**, using 1.2 equiv of TEMPO[•] in MeCN at room temperature for 10 min (eq 3). The TEMPO-H byproduct is

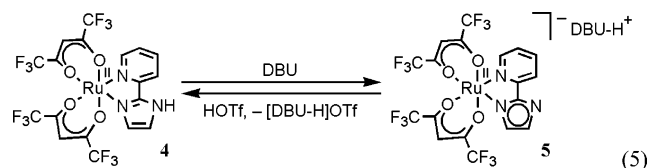


removed by sublimation, and **3** is isolated as a dark-brown solid in 65% yield. **3** can also be generated by the reaction of **2** with 1 equiv of the base DBU (1,8-diazabicyclo[5.4.0]-undec-7-ene) in MeCN (eq 4), but this is less convenient for preparative scale reactions. The addition of HOTf reprotonates **3** to form **2** (eq 4).



Related Ru^{II} -hexafluoro-acac derivatives are accessible starting from *cis*- $\text{Ru}^{\text{II}}(\text{hfac})_2(\text{MeCN})_2$.¹⁵ Refluxing this compound with 1.7 equiv of py-imH in C_6H_6 for 16 h yields $\text{Ru}^{\text{II}}(\text{hfac})_2(\text{py-imH})$ (**4**), analogous to eq 1. Red-brown **4** was obtained in 27% yield after silica gel chromatography.

Unreacted *cis*- $\text{Ru}^{\text{II}}(\text{hfac})_2(\text{MeCN})_2$ (21%) was also eluted from the column, but extending the reaction time or increasing the amount of py-imH (up to 10 equiv) did not improve the yield of **4**. The addition of 1 equiv of DBU immediately deprotonates **4** in MeCN to generate $[\text{DBU-H}][\text{Ru}^{\text{II}}(\text{hfac})_2(\text{py-im})]$ (**5**), which was isolated as a black-purple solid in 76% yield (eq 5). Spectroscopic and X-ray characterizations of these compounds are presented in the next sections, and all of the structures and compound numbers are shown in Scheme 2 below.



X-ray Structures. X-ray crystal structures of **1–5** have been solved. ORTEP drawings of each ruthenium complex (with 50% probability ellipsoids) are shown in Figures 1 and 2, and the crystallographic and metrical data are given in Tables 1 and 2. The ruthenium complexes all have very similar distorted octahedral geometries, with trans angles $> 170^\circ$. The py-imH ligands form five-membered chelate rings with small bite angles of $78.4(3)–79.6(3)^\circ$. The Ru–O bond lengths are all quite similar for the three Ru^{II} complexes **1**, **4**, and **5** (2.026(7)–2.056(6) Å), independent of whether the ligand is acac or hfac. The oxidized compounds **2** and **3** have slightly shorter Ru–O distances of 1.995(4)–2.017(4) Å. These values are typical of related compounds.^{20,21} In **1**, the $\text{Ru}^{\text{II}}\text{–N}(\text{imidazole})$ bond is 0.029(10) Å longer than the $\text{Ru}^{\text{II}}\text{–N}(\text{py})$ bond, but this is reversed in the Ru^{III} complexes **2** and **3**, where the bonds to the imidazole or imidazolate are 0.036(7) and 0.045(9) Å shorter. This presumably reflects the greater π -backbonding for $\text{Ru}^{\text{II}} \rightarrow \text{py}$. This is also evident with the more electron-deficient hfac complex **4**, which has less π -backbonding and thus has similar Ru–N(py) and Ru–N(imidazole) distances. Deprotonation of the imidazole

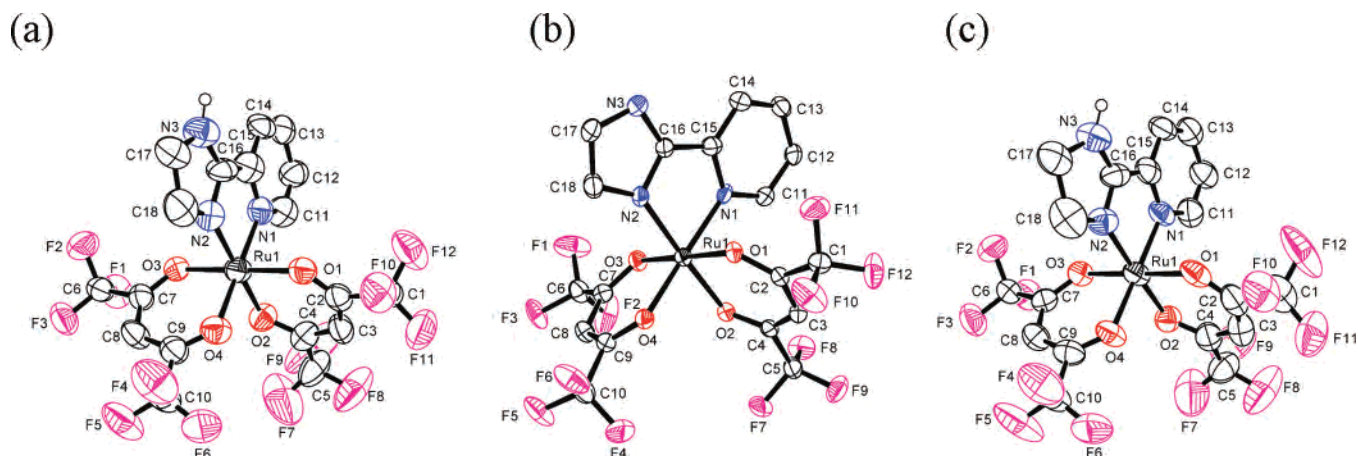


Figure 2. ORTEP drawings of (a) $\text{Ru}^{\text{II}}(\text{hfac})_2(\text{py-imH})$ (**4**), (b) $[\text{Ru}^{\text{II}}(\text{hfac})_2(\text{py-im})]^-$ (**5**), and (c) $\text{Ru}^{\text{II}}(\text{hfac})_2(\text{py-immH})$ (**8**) (see below), showing one of the two independent molecules in the unit cell for each of **4** and **8**. Hydrogen atoms are omitted for clarity except for the N–H atom.

Table 1. X-ray Crystallographic Data for **1–5** and **8**

	$1 \cdot 0.5\text{C}_6\text{H}_6$	$[2]_2 \cdot \text{CH}_2\text{Cl}_2$	3	4	5	8
empirical formula	$\text{C}_{21}\text{H}_{24}\text{N}_3\text{O}_4\text{Ru}$	$\text{C}_{39}\text{H}_{44}\text{N}_6\text{O}_{14}\text{Cl}_2\text{F}_6\text{S}_2\text{Ru}_2$	$\text{C}_{18}\text{H}_{20}\text{N}_3\text{O}_4\text{Ru}$	$\text{C}_{18}\text{H}_6\text{N}_3\text{O}_4\text{F}_{12}\text{Ru}$	$\text{C}_{27}\text{H}_{25}\text{N}_5\text{O}_4\text{F}_{12}\text{Ru}$	$\text{C}_{18}\text{H}_{11}\text{N}_3\text{O}_4\text{F}_{12}\text{Ru}$
fw	483.50	1271.96	443.44	660.35	812.40	662.37
cryst syst	monoclinic	triclinic	monoclinic	triclinic	triclinic	monoclinic
space group	$P2_1/c$	$P\bar{1}$	$P2_1/c$	$P2_1/c$	$P\bar{1}$	$P2_1/c$
a (Å)	7.5358(6)	7.6240(6)	10.2674(5)	9.8590(4)	10.9792(3)	9.87150(10)
b (Å)	15.9357(14)	11.7300(7)	11.4128(6)	19.4590(10)	12.3770(4)	19.7664(3)
c (Å)	17.595(2)	14.9360(11)	15.8465(10)	23.8400(13)	12.6990(5)	23.8995(4)
α (deg)	90	112.531(3)	90	90	89.131(1)	90
β (deg)	106.260(3)	95.165(3)	90.087(3)	90.390(2)	80.044(2)	90.4656(5)
γ (deg)	90	94.249(3)	90	90	65.729(2)	90
V (Å ³)	2028.5(3)	1220.17(15)	1856.89(18)	4573.5(4)	1546.43(9)	4663.21(12)
Z	4	1	4	8	2	8
d_{calcd} (g/cm ³)	1.583	1.731	1.586	1.918	1.745	1.887
μ (mm ⁻¹)	0.806	0.906	0.872	0.815	0.622	0.800
λ (Å)	0.71073	0.71073	0.71073	0.71073	0.71073	0.71073
cryst size (mm ³)	$0.24 \times 0.17 \times 0.12$	$0.29 \times 0.20 \times 0.01$	$0.59 \times 0.59 \times 0.48$	$0.24 \times 0.10 \times 0.08$	$0.40 \times 0.40 \times 0.20$	$0.48 \times 0.26 \times 0.24$
T (K)	130(2)	130(2)	130(2)	130(2)	130(2)	130(2)
θ range (deg)	2.41–25.49	2.70–25.45	2.20–28.32	2.09–28.31	2.07–30.02	2.06–28.29
index ranges	$-9 \leq h \leq 9$ $-19 \leq k \leq 19$ $-21 \leq l \leq 21$	$-9 \leq h \leq 8$ $-14 \leq k \leq 14$ $-18 \leq l \leq 18$	$-12 \leq h \leq 13$ $-14 \leq k \leq 14$ $-17 \leq l \leq 21$	$-13 \leq h \leq 13$ $-23 \leq k \leq 25$ $-31 \leq l \leq 31$	$-15 \leq h \leq 13$ $-16 \leq k \leq 13$ $-17 \leq l \leq 14$	$-13 \leq h \leq 13$ $-26 \leq k \leq 24$ $-31 \leq l \leq 31$
reflns collected	6807	7785	11 848	18 527	10 219	19 246
unique reflns	3652	4479	4276	10 787	6954	10 926
R_{int}	0.0992	0.0520	0.0688	0.1274	0.0713	0.0325
params refined	267	330	239	685	470	685
$R1, wR2$ ($I > 2\sigma(I)$)	0.0649, 0.1649	0.0580, 0.1669	0.0653, 0.1939	0.0768, 0.1993	0.0609, 0.1440	0.0601, 0.1736
GOF	0.984	1.051	1.021	0.917	1.041	1.010

Table 2. Selected Bond Lengths (Angstroms) and Angles (Degrees) in the X-ray Structures of **1–5** and **8**

	1	2	3	4^a	5	8^a
Ru1–O1	2.031(6)	1.997(4)	2.002(4)	2.026(7)	2.026(3)	2.035(4)
Ru1–O2	2.046(6)	2.006(4)	2.012(4)	2.041(6)	2.042(3)	2.036(4)
Ru1–O3	2.056(6)	1.997(4)	1.995(4)	2.042(6)	2.039(3)	2.047(3)
Ru1–O4	2.044(6)	2.005(4)	2.017(4)	2.028(7)	2.036(3)	2.032(3)
Ru1–N1	2.004(7)	2.063(5)	2.039(6)	2.023(8)	2.053(4)	2.039(4)
Ru1–N2	2.033(7)	2.027(5)	1.994(6)	2.024(8)	2.014(4)	2.015(5)
O1–Ru1–O2	94.0(2)	92.98(16)	91.92(18)	93.4(3)	94.33(12)	93.09(16)
O3–Ru1–O4	92.7(2)	90.73(17)	92.97(18)	93.5(3)	93.50(12)	92.99(13)
N1–Ru1–N2	79.2(3)	79.2(2)	78.4(3)	79.6(3)	79.14(14)	78.77(18)
O1–Ru1–O3	178.9(3)	178.87(16)	179.15(17)	179.5(3)	178.54(12)	179.71(14)
O4–Ru1–N1	175.7(2)	173.78(18)	173.4(2)	175.9(3)	171.13(12)	174.70(16)
O2–Ru1–N2	176.3(3)	175.73(17)	174.2(2)	174.1(3)	175.34(14)	173.89(16)

^a Data are for one of the two independent molecules in the unit cell.

ligand shortens its bond to ruthenium, in both **3** and **5**, as is typical for transition-metal imidazole complexes.²² The imidazole ligands of **1**, **2**, **4**, and **5** engage in various hydrogen bonding interactions in the crystals. In **1** and **4**,

there are intermolecular hydrogen bonds between imidazole N3–H and acac-oxygens ($d_{\text{N–O}} = 2.806\text{--}2.913$ Å) while in **2**, the imidazole N3–H bonds with the OTf^- counterion ($d_{\text{N–O}} = 2.747$ Å). The deprotonated imidazolite N3 in **5**

hydrogen bonds the acidic proton of DBU–H⁺ with $d_{N-N} = 2.746 \text{ \AA}$. These hydrogen bonding distances are within the typical range of 2.5–3.2 Å.²³

Spectroscopic Characterization. The ¹H NMR spectra of **1–5** in CD₃CN are consistent with the solid-state structures. For instance, the spectrum of diamagnetic **1** shows two inequivalent acac ligands [$\delta(\text{CH}_3)$ 2.05, 2.00, and 1.51 (2CH₃); $\delta(\text{CH})$ 5.32, 5.29], six pyridine–imidazole–CH signals (δ 7.09–8.75), and an imidazole–NH peak at δ 11.31 (which was confirmed by the exchange with CD₃OD). The Ru^{II} bis-hfac complexes **4** and **5** show similar proton resonances except for the absence of CH₃ peaks and a N–H signal for **5**. The ¹⁹F NMR spectra of **4** and **5** show four singlets between δ –74.74 and –75.06 (referenced to CF₃C(O)OH at δ –78.50),²⁴ consistent with the four inequivalent CF₃ groups. The ¹³C{¹H} NMR spectra of **4** and **5** in CD₃OD²⁵ show resonances for pyridine–imidazole (δ 118–168) and hfac–CH (δ 92–94) and four quartets for each of hfac–CF₃ (δ 117–120, ¹J_{CF} = 282 Hz) and hfac–C(O) (δ 165–173, ²J_{CF} = 33 Hz), again consistent with molecular C₁ symmetry.

The ¹H NMR spectra of paramagnetic complexes **2** and **3** (low-spin d⁵) in CD₃CN span a wide range, from δ 6 to –65 for **2** and δ 9 to –48 for **3** (Figure 3). The four acac–methyl resonances for **2** (δ –22 to –17) and **3** (δ –18 to –5) are assigned on the basis of integration. The imidazole–NH signal of **2** at δ 5.71 was identified by its exchange with added CD₃OD. ¹H 2D COSY NMR spectra (Figure S1 for **2** and Figure S2 for **3**, in the Supporting Information), which have previously been useful for paramagnetic assignments,²⁶ show cross-peaks for three of the four pyridine resonances in each spectrum of **2** and **3** (peak 1 couples to peaks 2 and 3 in Figure 3). The other couplings were not observed, likely

due to the paramagnetic broadening, which lowers the signal intensity and renders even the COSY diagonal peaks unobservable. The fourth pyridine resonances are tentatively assigned based on their proximity in chemical shift with the other three pyridine signals, but the other signals for **2** and **3** could not be assigned.

The correspondences between the resonances of **2** and **3** are shown by ¹H NMR titration in CD₃CN. The addition of 1 equiv of HOTf (pK_a = 2.60)²⁷ in 0.1 equiv increments to a solution of **3** gradually changes the spectrum of **3** into that of **2**, with the growth of the imidazole–NH signal (δ 5.71). **2** can be reversibly titrated back to **3** with 1 equiv of DBU (pK_a(DBU–H⁺) = 24.32²⁸). Proton exchange between **2** and **3** is thus fast on the NMR time scale, so that solutions containing both complexes show an averaged spectrum. This and related self-exchange reactions will be discussed in a future publication.²⁹

UV–vis spectra of **1**, **4**, and **5** all show strong MLCT bands in the visible region ($\epsilon = 6700\text{--}11\,000 \text{ M}^{-1} \text{ cm}^{-1}$, Figure 4), as is typical of Ru^{II}–pyridyl complexes.^{16,20b,30,31} As expected, the trend in the lowest MLCT energies, **1** < **5** < **4**, follows the ease of oxidation (below). However, the energies for **1** and **5** are quite close despite their 0.57 V difference in reduction potentials, and the two MLCT bands for **1** are much more widely spaced than those for the hfac analogue **4**. The Ru^{III} complexes **2** and **3** have much weaker charge-transfer transitions ($\epsilon = 2000, 1600 \text{ M}^{-1} \text{ cm}^{-1}$).

Electron impact mass spectra (EI/MS) of **1**, **2**, and **3** are indistinguishable in the positive-ion mode, each showing a mass cluster peaked at 444 *m/z*, which matches the simulated isotopic pattern for [Ru(acac)₂(py-im)]⁺. Thus, **1** and **2** are deprotonated in the process of obtaining EI/MS, and **1** is oxidized. With electrospray ionization (ESI) in MeCN, **2** and **3** show the protonated ion [Ru(acac)₂(py-imH)]⁺, centered at 445 *m/z*. (The air-sensitivity of **1** precludes its analysis by ESI/MS.) Positive-ion ESI/MS of **4** and **5** similarly show an isotopic pattern, which matches the oxidized protonated species [Ru(hfac)₂(py-imH)]⁺ (661 *m/z*). **5** also shows, in the negative-ion ESI/MS, a cluster at 660 *m/z* for the parent anion [Ru(hfac)₂(py-im)][–].

Thermochemical Measurements. (i) Cyclic Voltammetry. Cyclic voltammograms (CVs) of **1–5** in MeCN all show chemically reversible waves. In each case, the anodic and cathodic currents (i_a and i_c) are equal within 10%. The peak separations ($E_{p,a} - E_{p,c}$) at a scan rate of 100 mV s^{–1} are close to those of ferrocene in the same solution (80–

- (20) (a) Ru^{II}(acac)₂(3-amino-6-(3,5-dimethylpyrazol-1-yl)-1,2,4,5-tetrazine): Nayak, A.; Patra, S.; Sarkar, B.; Ghumaan, S.; Puranik, V. G.; Kaim, W.; Lahiri, G. K. *Polyhedron*, **2005**, *24*, 333. (b) *cis*- and *trans*-Ru^{II}(acac)₂L₂, [Ru^{III}(acac)₂(L)](ClO₄), and *trans*-[Ru^{III}(acac)₂(L)]₂(ClO₄) (L = 2,2'-dipyridylamine): Kar, S.; Chanda, N.; Mobin, S. M.; Urbanos, F. A.; Niemeyer, M.; Puranik, V. G.; Jimenez-Aparicio, R.; Lahiri, G. K. *Inorg. Chem.* **2005**, *44*, 1571. (c) Ru^{II}(acac)₂(*o*-benzoquinonediimine) and Ru^{II}(acac)₂(*N*-phenyl-1,2-benzoquinone-diimine): Mitra, K. N.; Choudhury, S.; Castideiras, A.; Goswami, S. *J. Chem. Soc., Dalton Trans.* **1998**, 2901.
- (21) Reported structures for Ru–hfac complexes: (a) *cis*-Ru^{II}(hfac)₂(MeCN)₂, *cis*-Ru^{II}(acac)(hfac)(MeCN)₂, Ru^{III}(hfac)₃: ref 15. (b) *cis*-Ru^{II}(hfac)₂(CO)₂: Lee, F.-J.; Chi, Y.; Liu, C.-S.; Hsu, P.-F.; Chou, T.-Y.; Peng, S.-M.; Lee, G.-H. *Chem. Vap. Deposition* **2001**, *7*, 99 (which reports slightly longer Ru–O distances, 2.050(2)–2.081(2) Å, compared to those in **4** and **5**). (c) *cis*- and *trans*-Ru^{III}Cl₂(hfac)₂(PPh₃)₂: Colson, S. F.; Robinson, S. D.; Robinson, P. D.; Hinckley, C. C. *Acta Crystallogr. C* **1989**, *45*, 715.
- (22) (a) Tadokoro, M.; Kanno, H.; Kitajima, T.; Shimada-Umemoto, H.; Nakinishi, N.; Isobe, K.; Nakasuji, K. *Proc. Natl. Acad. Sci. U.S.A.* **2002**, *99*, 4950. (b) Mandon, D.; Ott-Woelfel, F.; Fischer, J.; Weiss, R.; Bill, E.; Trautwein, A. X. *Inorg. Chem.* **1990**, *29*, 2442. (c) Mayboroda, A.; Comba, P.; Pritzkow, H.; Rheinwald, G.; Lang, H.; van Koten, G. *Eur. J. Inorg. Chem.* **2003**, 1703.
- (23) Jeffrey, G. A. *An Introduction to Hydrogen Bonding*; Oxford University Press: New York, 1997.
- (24) Walstrom, A.; Pink, M.; Tsvetkov, N. P.; Fan, H.; Ingleson, M.; Caulton, K. G. *J. Am. Chem. Soc.* **2005**, *127*, 16780; supporting information.
- (25) CD₃OD is used in ¹³C{¹H} NMR instead of CD₃CN because the latter solvent has a resonance at δ 118 that significantly overlaps with the low-intensity quartets of hfac–CF₃.

- (26) (a) Kennedy, D. C.; Wu, A.; Patrick, B. O.; James, B. R. *Inorg. Chem.* **2005**, *44*, 6529. (b) Belle, C.; Bougault, C.; Averbuch, M.-T.; Durif, A.; Pierre, J.-L.; Latour, J.-M. Le Pape, L. *J. Am. Chem. Soc.* **2001**, *123*, 8053. (c) Bertini, I.; Capozzi, F.; Luchinat, C.; Turano, P. *J. Magn. Reson.* **1991**, *95*, 244.
- (27) Izutsu, K. *Acid-Base Dissociation Constants in Dipolar Aprotic Solvents*; Blackwell Scientific: Boston, 1990.
- (28) Schwesinger, R.; Schlemper, H. *Angew. Chem., Int. Ed. Engl.* **1987**, *26*, 1167.
- (29) Wu, A.; Mayer, J. M., to be submitted.
- (30) Ghumaan, S.; Sarkar, B.; Patra, S.; Parimal, K.; van Slageren, J.; Fiedler, J.; Kaim, W.; Lahiri, G. K. *J. Chem. Soc., Dalton Trans.* **2005**, 706.
- (31) Seddon, E. A.; Seddon, K. R. *The Chemistry of Ruthenium*; Elsevier: Amsterdam, The Netherlands, 1984; p 474.

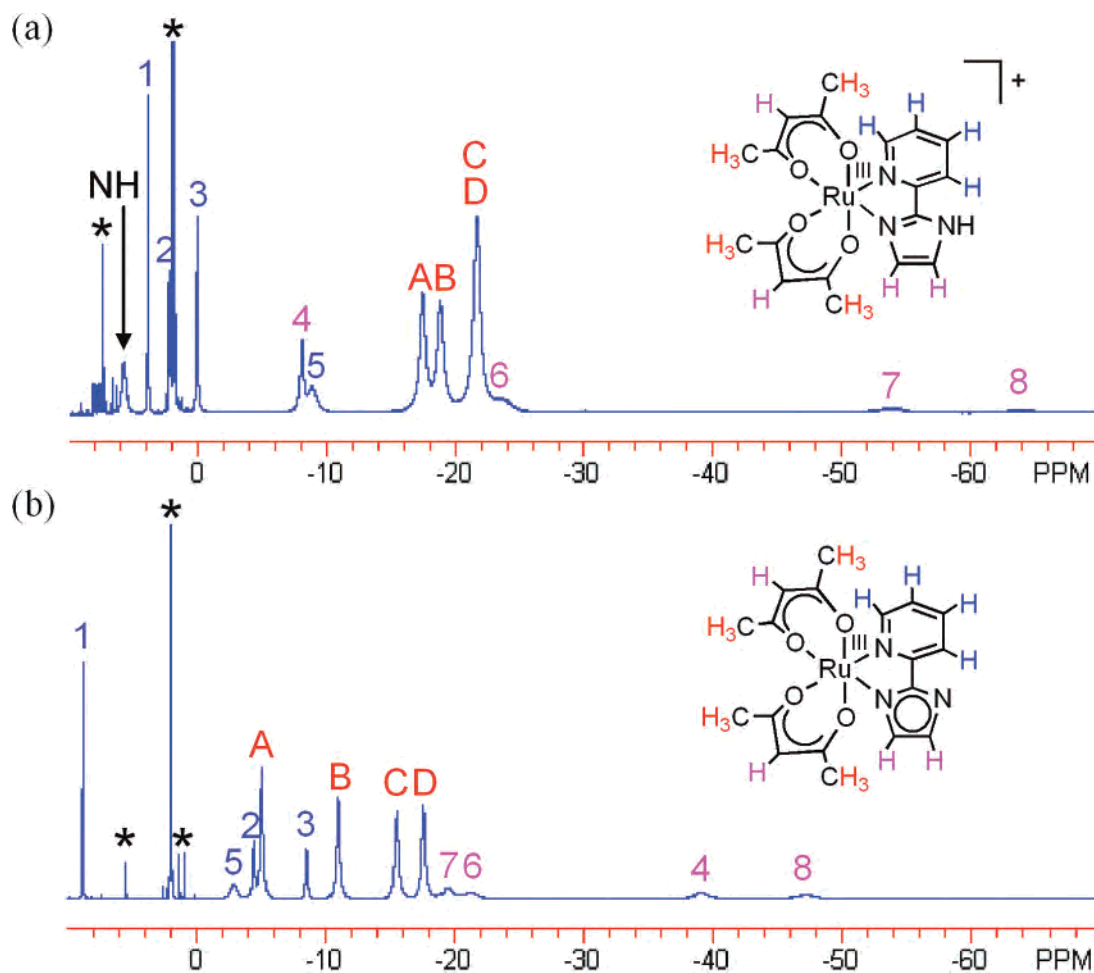


Figure 3. ^1H NMR spectra of (a) $[\text{Ru}^{\text{III}}(\text{acac})_2(\text{py-imH})]\text{OTf}$ (**2**) and (b) $\text{Ru}^{\text{III}}(\text{acac})_2(\text{py-im})$ (**3**) in CD_3CN . Peaks A to D are assigned as acac- CH_3 protons, peaks 1, 2, 3, and 5 as pyridine protons, and 4, 6, 7, and 8 as acac- or imidazole- CH protons. The letters and numbers show the corresponding signals between **2** and **3**, as determined by reversible NMR titration by DBU/HOTf. Solvent and impurity peaks are denoted by asterisks (*).

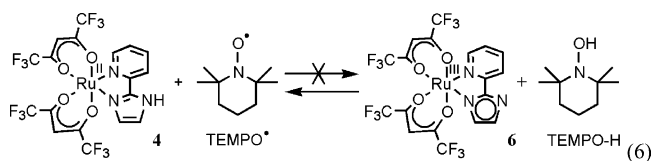
100 mV), but at higher scan rates the ruthenium complexes show larger separations (up to 40 mV larger). The waves correspond to the $\text{Ru}^{\text{III/II}}$ redox couples. $E_{1/2}$ for **1** and **2** is at -0.64 V, which shifts to -1.00 V upon deprotonation to form **3** (potentials ± 0.01 V in MeCN referenced to internal $\text{Cp}_2\text{Fe}^{+/0}$). The hfac compounds are 0.93 V more difficult to oxidize: $E_{1/2} = 0.29$ (**4**) and -0.07 V (**5**). In both the acac and hfac compounds, the protonated form (**1**, **2**, or **4**) has a higher reduction potential than the deprotonated species (**3** or **5**) by 0.36 V.

(ii) pK_a Values. The interconversion of protonated **2** and deprotonated **3** in MeCN by 1 equiv of DBU or HOTf (eq 4 above) was monitored by optical spectroscopy, confirming the ^1H NMR results described above. Titration of **2** with an excess of the weak base 2,4-lutidine ($pK_a(2,4\text{-lutidine-H}^+) = 14.05$)²⁷ forms **3** in an equilibrium. With concentrations of **2** and **3** determined from optical spectra (Figure 4), the equilibrium constant for $\text{2} + 2,4\text{-lutidine} \rightleftharpoons \text{3} + (2,4\text{-lutidine-H})\text{OTf}$ was determined to be 0.011 ± 0.001 from the slope of the linear plot: $[\text{3}][2,4\text{-lutidine-H}^+]/[\text{2}]$ vs $[2,4\text{-lutidine}]$ (Figure S3 in the Supporting Information and in the Experimental Section). This K_{eq} and the pK_a of 2,4-lutidine- H^+ give $pK_a(\text{2}) = 16.0 \pm 0.1$. Similarly, UV-vis monitoring shows quantitative interconversion of the Ru^{III}

hfac derivatives **4** and **5** with DBU and HOTf (eq 5). Titration of **4** with Et_3N ($pK_a(\text{Et}_3\text{NH}^+) = 18.46$)²⁷ gives a pK_a of 19.3 ± 0.1 for **4**.

Hydrogen Atom Transfer Reactions of the Imidazole/Imidazolate Complexes with TEMPO $^\bullet$ /TEMPO-H. Complex **1** in CD_3CN is rapidly oxidized by 1 equiv of TEMPO $^\bullet$ at ambient temperatures to produce **3** and TEMPO-H³² (eq 3 above). This reaction has been monitored by optical and ^1H NMR spectroscopies and is evident by the solution color changing from the red-purple of **1** to the pale-brown of **3**. This and related hydrogen atom transfer (HAT) reactions in the $\text{Ru}(\text{acac})_2$ system will be described in detail in a future publication, including HAT self-exchange reactions and kinetic isotope effects.²⁹

The hfac analogue **4**, however, does not react with 36 equiv of TEMPO $^\bullet$ in CD_3CN at room temperature under N_2 after 1 d (eq 6). To understand this lack of reactivity, the



expected product, $\text{Ru}^{\text{III}}(\text{hfac})_2(\text{py-im})$ (**6**), was generated in

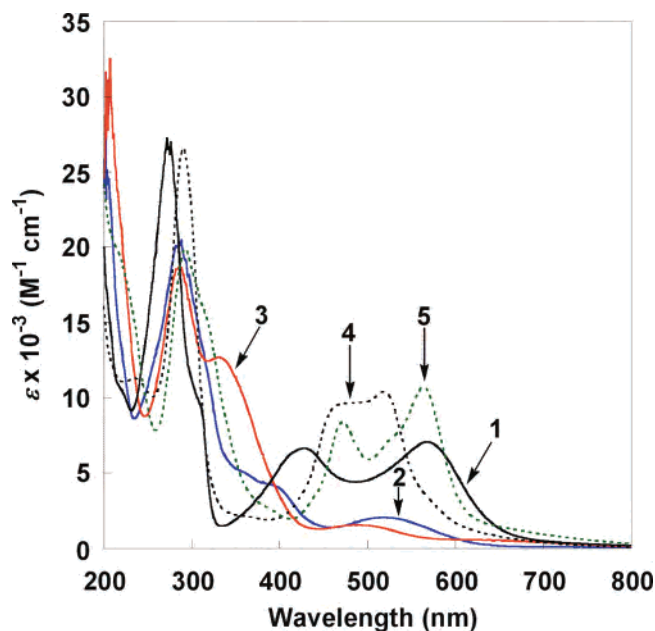
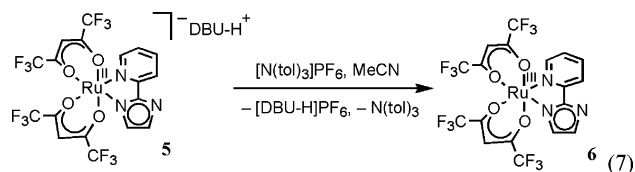


Figure 4. UV-vis spectra of Ru^{II}(acac)₂(py-imH) (**1**), [Ru^{III}(acac)₂(py-imH)]OTf (**2**), Ru^{III}(acac)₂(py-im) (**3**), Ru^{II}(hfac)₂(py-imH) (**4**), and [DBU-H][Ru^{II}(hfac)₂(py-im)] (**5**) in MeCN.

situ by the oxidation of **5** with 1 equiv of tri-*p*-tolylammonium hexafluorophosphate ([N(tol)₃]⁺PF₆⁻, $E_{1/2} = 0.38$ V vs Cp₂Fe⁺⁰)³³ (eq 7). Monitoring reaction 7 by UV-vis spec-



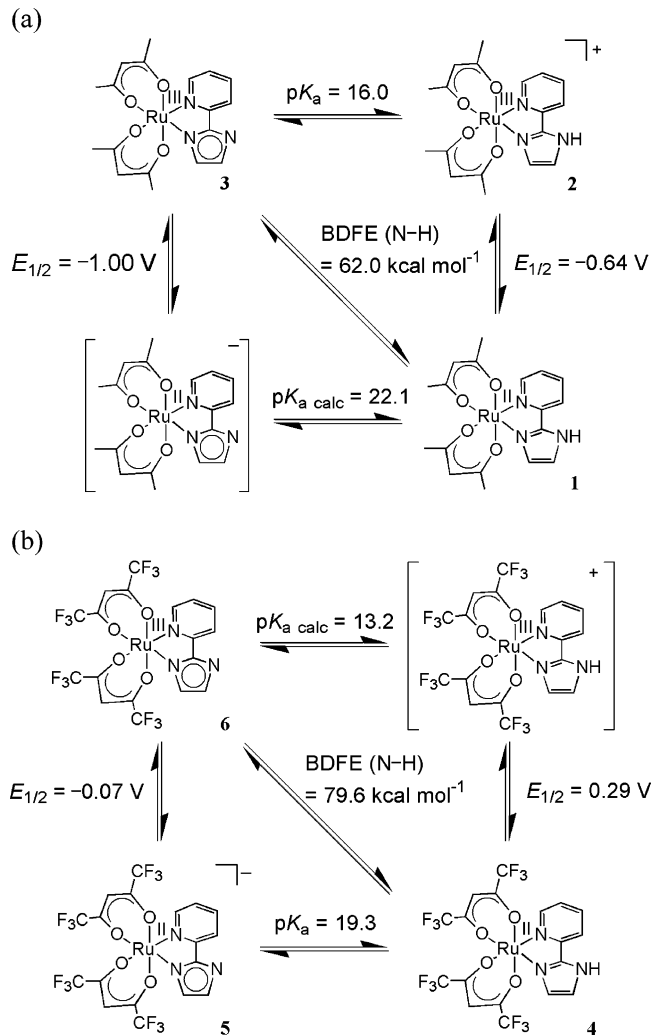
troscopy shows an isosbestic point at 450 nm up to 1 equiv of [N(tol)₃]⁺PF₆⁻ (Figure S4). Beyond 1 equiv, the absorbance due to [N(tol)₃]⁺PF₆⁻ at $\lambda_{\max} = 668$ nm ($\epsilon = 26\,200$ M⁻¹ cm⁻¹)³⁴ grows in. By ¹H NMR, the addition of 1 equiv of [N(tol)₃]⁺PF₆⁻ in CD₃CN causes the disappearance of the resonances of **5**, but no resonances for paramagnetic **6** are observed. The CV of this in situ-generated **6** shows a reversible wave with $E_{1/2} = -0.07$ V, identical to that of **5**. Complex **6** appears to slowly decay in solution, as small amounts of the Ru^{II} protonated complex **4** are observed by NMR after ~20 min at room temperature under N₂. Attempts to isolate **6** by reprecipitation with CH₂Cl₂/*n*-pentane under N₂ lead to the isolation of **4**. In situ-prepared **6** reacts rapidly with 1 equiv of TEMPO-H to quantitatively form **4** (eq 6), as monitored by ¹H NMR and UV-vis (Figure S4, in the Supporting Information) spectroscopies. The lack of reaction of **4** with TEMPO[•] thus has a thermochemical, rather than a kinetic origin (see below).

(32) Ref 7c: supporting information.

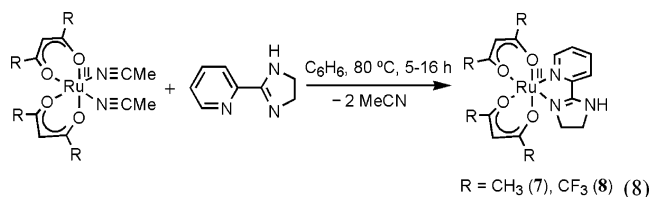
(33) (a) Bandlish, B. K.; Shine, H. J. *J. Org. Chem.* **1977**, *42*, 561. (b) Ebersson, L.; Larsson, B. *Acta Chem. Scand., Ser. B* **1986**, *40*, 210. (c) Rhile, I. J.; Markle, T. F.; Nagao, H.; DiPasquale, A. G.; Lam, O. P.; Lockwood, M. A.; Rotter, K.; Mayer, J. M. *J. Am. Chem. Soc.* **2006**, *128*, 6075 and references therein.

(34) Gould, I. R.; Ege, D.; Moser, J. E.; Farid, S. *J. Am. Chem. Soc.* **1990**, *112*, 4290.

Scheme 2. Square Schemes for (a) the Ru-acac-py-imH (**1–3**) and (b) the Ru-hfac-py-imH (**4–6**) Systems (in MeCN at 298 K, $E_{1/2}$ Values vs Cp₂Fe⁺⁰).



Imidazoline Complexes and Their Reactions with TEMPO[•]. Prior to studying the pyridine-imidazole complexes above, we explored complexes of the partially saturated analogue, 2-(2'-pyridyl)imidazoline (py-imnH).³⁵ Analogous to the procedures used for **1** and **4**, Ru^{II}(acac)₂(py-imnH) (**7**) and Ru^{II}(hfac)₂(py-imnH) (**8**) were synthesized from the bis(acetonitrile) derivatives (eq 8).

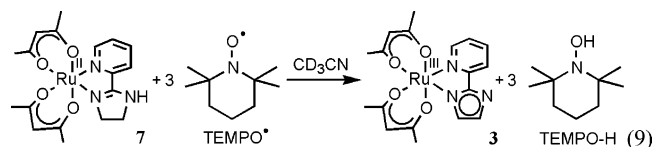


The X-ray structure of the hfac-imidazoline complex **8** (part c of Figure 2) is similar to that of the imidazole analogue **4**, but the saturated imidazoline C–C bond (1.591(10) Å) is longer than the imidazole C=C bond (1.443(14) Å). **7** has a ¹H NMR spectrum analogous to that of **1** except

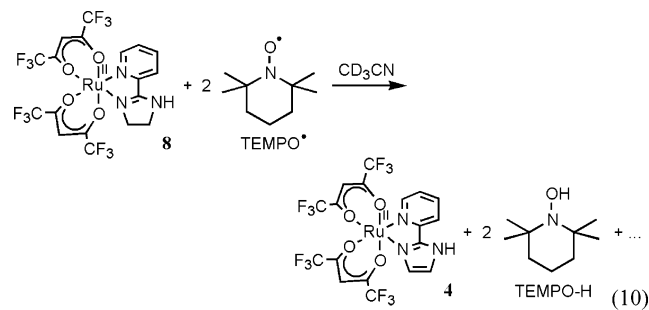
(35) Mohammadpoor-Baltork, I.; Abdollahi-Alibeik, M. *Bull. Korean Chem. Soc.* **2003**, *24*, 1354.

that the imidazoline CH₂ multiplets (δ 3.6–4.0) and NH singlet (δ 6.12) are shifted more upfield than the aromatic imidazole CH (δ 7–8) and NH signals (δ 11.31), as expected. The hfac complexes **8** and **4** show the same pattern. The ¹³C{¹H} NMR spectrum of **8** in CD₃OD shows resonances similar to those of **4** and **5**, except that the imidazoline C–H peaks (δ 46.12, 55.58) are more upfield than those of the imidazole (δ 121–133). Cyclic voltammetry of the imidazoline complexes gives Ru^{III/II} $E_{1/2}$ values of –0.68 for **7** and 0.14 V for **8**. Complexes **7** and **8** are slightly easier to oxidize than their imidazole analogues **1** and **4**, by 0.04 and 0.15 V, respectively.

The Ru^{II}–acac–imidazoline complex **7** in CD₃CN reacts slowly with 3 equiv of TEMPO• at room temperature under N₂ to give the imidazolate complex **3** and TEMPO–H (eq 9), as monitored by ¹H NMR. The formation of **3**



involves removal of *three* hydrogen atoms from the imidazoline ring, one from the NH, and one from each of the methylene groups. Such dehydrogenation of imidazoline has not been observed in any of the iron chemistry we have explored,^{6a,b,7} but oxidation of coordinated amines is well-known for ruthenium complexes.³⁶ This dichotomy may be a result of the dehydrogenation requiring M^{IV} intermediate(s), which are accessible for Ru^{IV} but too high in energy for Fe^{IV}.³⁶ Reaction 9 does not proceed quantitatively, but with 10 equiv of TEMPO•, a yield of 72% of **3** is observed by ¹H NMR after 1 d. The hfac analogue **8** also reacts slowly with 10 equiv of TEMPO• in CD₃CN at room temperature under N₂ to aromatize the imidazoline ligand, but in this case the Ru^{II}–protonated complex **4** is formed in 50% yield after 4 d (eq 10), with some starting **8** (14%) still remaining.



Discussion

I. Bond Dissociation Free Energies (BDFEs) of **1 and **4**.** The thermochemical data above can be assembled into square schemes² that are thermochemical maps of the ruthenium acac–imidazole and hfac–imidazole systems (Scheme 2). The horizontal equilibrium arrows give the p*K*_a values, the verticals give the $E_{1/2}$ potentials, and the diagonals are the bond dissociation free energies (BDFEs) for HAT.

BDFEs are derived from the p*K*_a and $E_{1/2}$ values using eq 11, where *R* is the gas constant, *T* is temperature, and *F* is

$$\text{BDFE} = 2.3RT\text{p}K_a + FE_{1/2} + C_G = [1.37\text{p}K_a + 23.1E_{1/2} + 54.9] \text{ kcal mol}^{-1} \quad (11)$$

the Faraday constant.³⁷ C_G is the free energy for $\text{H}^+_{\text{MeCN}} + e^- \rightarrow \text{H}^{\bullet}_{\text{MeCN}}$. It has been given by Tilset^{37a} as the sum of $F[E^\circ(\text{Cp}_2\text{Fe}^{+/0}) - E^\circ(\text{H}^+/\text{H}_2)]$ (equal to 1.2 kcal mol^{–1}),³⁸ the free energy of formation of H• in the gas phase [$\Delta G^\circ_{\text{f}}(\text{H}^{\bullet})_{\text{g}} = 48.6 \text{ kcal mol}^{-1}$],³⁹ and the free energy of solvation of H• ($\Delta G^\circ_{\text{solv}}(\text{H}^{\bullet})_{\text{MeCN}} = 5.1 \text{ kcal mol}^{-1}$).⁴⁰ Thus, C_G in MeCN with potentials referenced to Cp₂Fe⁺⁰ is equal to 54.9 kcal mol^{–1}.³⁷ Using eq 11, this value of C_G , the p*K*_a of **2** and the $E_{1/2}$ for **3** give the BDFE of the N–H bond in **1** to be 62.0 ± 1.0 kcal mol^{–1} in MeCN at 298 K.⁴¹ Similarly, the BDFE of **4** is calculated to be 79.6 ± 1.0 kcal mol^{–1}, using the p*K*_a of **4** and $E_{1/2}$ of **5**.

The four outside edges of the square scheme also form a thermochemical cycle, so the sum of these four terms (in free-energy terms) must equal to zero (eq 12). For both the

$$1.37[\text{p}K_a(\mathbf{1}) - \text{p}K_a(\mathbf{2})] + 23.1[E_{1/2}(\mathbf{3}) - E_{1/2}(\mathbf{2})] = 0 \quad (12)$$

acac and hfac systems, two reduction potentials and one p*K*_a have been measured, so eq 12 enables calculation of the second p*K*_a: 22.1 ± 0.3 for **1** and 13.2 ± 0.3 for [Ru^{III}–(hfac)₂(py–imH)]⁺.

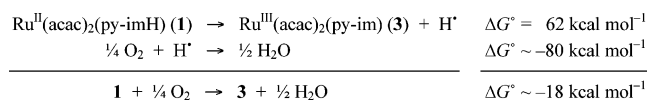
II. Thermochemistry and Reactivity. The thermochemical measurements are consistent with the observed reactivity of the ruthenium complexes with TEMPO• and TEMPO–H. The O–H BDFE of TEMPO–H is 66.5 ± 1.1 kcal mol^{–1}.^{7b} The reaction of **1** plus TEMPO• to give **3** and TEMPO–H therefore has $\Delta G^\circ_3 = -4.5 \pm 0.9 \text{ kcal mol}^{-1}$ [= BDFE(**1**) – BDFE(TEMPO–H)]⁴² and $K_{\text{eq}} \cong 2 \times 10^3$. This agrees with the experimental observation that **1** + TEMPO• proceeds to completion, as monitored by ¹H NMR (eq 3). The calculated free energy for the reaction of hfac complex **4** with TEMPO• (eq 6) is strongly unfavorable, $\Delta G^\circ_6 = +13.1 \pm 0.9 \text{ kcal mol}^{-1}$. This is consistent with the lack of observed reactivity in the forward direction and the facile reaction in the opposite direction: **6** + TEMPO–H → **4** + TEMPO•.

The Ru^{II} acac complexes **1** and **7** are air-sensitive because they are reducing and have relatively weak N–H bonds. Stirring a solution of **1** in MeCN under air produces mainly the Ru^{III} deprotonated complex **3**. The mechanism of reaction

- (37) (a) Tilset, M. In *Electron Transfer in Chemistry*; Balzani, V., Ed.; Wiley-VCH: Weinheim, Germany, 2001; Vol. 2, pp 677–713. (b) Parker, V. D.; Handoo, K. L.; Roness, F.; Tilset, M. *J. Am. Chem. Soc.* **1991**, *113*, 7493. (c) Ref 37a gives $C_G = 54.9 \text{ kcal mol}^{-1}$ for cycles in MeCN with reduction potentials referenced to Cp₂Fe⁺⁰ (p. 681), whereas ref 37b gives $C_G = 53.7 \text{ kcal mol}^{-1}$ for cycles in MeCN with reduction potentials referenced to H⁺/H₂ in MeCN.
- (38) Kolthoff, I. M.; Chantooni, M. K., Jr. *J. Phys. Chem.* **1972**, *76*, 2024.
- (39) *CRC Handbook of Chemistry and Physics*, 67th ed.; Weast, R. C., Ed.; CRC Press: Boca Raton, FL, 1986–1987; p D-69.
- (40) Brunner, E. *J. Chem. Eng. Data* **1985**, *30*, 269.
- (41) The estimated error in the BDFE is predominantly from the uncertainty in C_G , which we estimate to be ±1 kcal mol^{–1}.³⁷
- (42) The relative error in ΔG° calculated from the difference between two BDFEs (determined with the same C_G) is less than the error of each BDFE because the uncertainty in C_G cancels itself out.

(36) Keene, F. R. *Coord. Chem. Rev.* **1999**, *187*, 121 and references therein.

Scheme 3



of **1** with O_2 could proceed by an initial electron transfer to give **2** and $\text{O}_2^{\bullet-}$ ($E = -0.46 \text{ V}$, $\Delta G^{\circ} = +11 \text{ kcal mol}^{-1}$), by initial HAT to give **3** + HO_2^{\bullet} ($\Delta G^{\circ} \cong +2 \text{ kcal mol}^{-1}$),⁴³ or by chain or base-catalyzed processes.⁴⁴ The overall reaction of **1** with O_2 is favorable by roughly 18 kcal per mole of ruthenium (Scheme 3). This is only an estimate because it uses the gas-phase value for $\frac{1}{4} \text{O}_2 + \text{H}^{\bullet} \rightarrow \frac{1}{2} \text{H}_2\text{O}$,⁴³ a proper analysis would use the value in the MeCN solution. The hfac complexes **4** and **8**, in contrast, are not air-sensitive at least in part because their reactions with O_2 are significantly less favorable: $\Delta G^{\circ} = \sim 0 \text{ kcal mol}^{-1}$ for **4** + $\frac{1}{4} \text{O}_2 \rightarrow \text{6} + \frac{1}{2} \text{H}_2\text{O}$.

The Ru^{III} hfac deprotonated complex **6** has eluded isolation because of its ease of reduction, whereas the acac analogue **3** is quite stable. **6** appears to decay at least in part due to reactions with trace impurities in the solvents used, despite various purification attempts. The sensitivity of **6** is apparently not due to its reduction potential, which at $E_{1/2} = -0.07 \text{ V}$ versus $\text{Cp}_2\text{Fe}^{+/0}$ is relatively modest, but rather seems to result from its ability to form a strong N–H bond (BDFE = $79.6 \text{ kcal mol}^{-1}$). We and others have been working with a variety of hydrogen atom abstractors,⁴⁵ and as a general rule of thumb, it is often difficult to isolate species that add H^{\bullet} to form a bond with a BDFE above ca. 80 kcal mol^{-1} . Converting this to the more commonly used bond dissociation enthalpy (BDE),^{7b} the borderline is ca. 85 kcal mol^{-1} . (For a given X–H bond, the BDE in MeCN is roughly $4.6 \text{ kcal mol}^{-1}$ larger than the BDFE, using the not-always-accurate assumption that $S^{\circ}(\text{X}) = S^{\circ}(\text{XH})$.^{7b})

III. Thermochemical Comparisons. Replacing two acac ligands with less-donating hfac ligands makes the metal less electron rich and raises the $\text{Ru}^{\text{III/II}}$ reduction potential. The difference is 0.93 V for both the protonated (**1**, **2** vs **4**) and deprotonated imidazole complexes (**3** vs **5**) and 0.82 V for the protonated imidazoline complexes (**7** vs **8**). Similar differences in $E_{1/2}$ have been reported for related acac/hfac pairs: $\Delta E_{1/2} = 0.88 \text{ V}$ ¹⁶ for $[\text{Ru}(\text{hfac}/\text{acac})_2(\text{bpy})]^{+/0}$ and 0.99 V for *cis*- $[\text{Ru}(\text{hfac}/\text{acac})_2(\text{MeCN})_2]^{+/0}$.^{15,46} The Lever parameters⁴⁷ predict a change of $E_{1/2}$ by 0.97 V between ruthenium bis-acac and bis-hfac complexes, in very good agreement with the observed $\Delta E_{1/2}$ for the bis-acetonitrile and imidazole complexes, but somewhat overestimating the change for the bpy and imidazoline species.

The acac complex **1** has a $17.6 \pm 0.4 \text{ kcal mol}^{-1}$ weaker N–H bond than the hfac derivative **4**.⁴² This is a dramatic difference in BDFEs. For comparison, replacing CH_3 for CF_3 in substituted toluenes, *p*- $\text{CH}_3\text{C}_6\text{H}_4\text{CH}_3$ versus *p*- $\text{CF}_3\text{C}_6\text{H}_4\text{CH}_3$, shifts the benzylic C–H bond dissociation enthalpies (BDE)⁴⁸ only by $0.9 \text{ kcal mol}^{-1}$ (for organic compounds,

$\Delta\text{BDE} \cong \Delta\text{BDFE}$ ^{7b}). For anilines and phenols, the differences are somewhat larger, for instance $\Delta\text{BDE} = 5.2 \text{ kcal mol}^{-1}$ for *p*- $\text{CH}_3\text{C}_6\text{H}_4\text{NH-H}$ versus *p*- $\text{CF}_3\text{C}_6\text{H}_4\text{NH-H}$.⁴⁸ In general, changes that make a compound less electron rich will raise the reduction potential and lower the $\text{p}K_{\text{a}}$ and therefore balance each other in terms of the BDFE (eq 11). Thus, the BDFE (and BDE) are less sensitive to substituent effects than either the $E_{1/2}$ or $\text{p}K_{\text{a}}$. Electron or proton transfer involves changes in charge and charge distribution, whereas homolytic X–H bond scission is to a first approximation a nonpolar process. This has been beautifully illustrated by DuBois et al. for nickel and palladium hydride complexes.⁴⁹ For $[\text{Pd}(\text{H})(\text{diphosphine})_2]^+$ complexes, varying the ligands shifts the redox potentials by 0.30 V (equivalent to 7 kcal mol^{-1}), whereas the $\text{p}K_{\text{a}}$ values shift by 4.7 units in the opposite direction, so that the BDFEs vary by only $0.7 \text{ kcal mol}^{-1}$.^{49a} In the related nickel system, the shift of 0.32 V in $E_{1/2}$ is more than offset by the $7 \text{ p}K_{\text{a}}$ unit shift, so that the more basic compounds have higher BDFEs by $2.0 \text{ kcal mol}^{-1}$.^{49b}

These examples illustrate that the $17.6 \pm 0.4 \text{ kcal mol}^{-1}$ shift between acac and hfac ruthenium complexes described here is particularly large. It occurs because the reduction potentials are much more affected than the $\text{p}K_{\text{a}}$ values: the $\Delta E_{1/2}$ of 0.93 V corresponds to $\Delta\Delta G^{\circ} = 21.4 \text{ kcal mol}^{-1}$ ($= F\Delta E_{1/2}$), whereas the $\Delta\text{p}K_{\text{a}}$ of 2.8 units is only $\Delta\Delta G^{\circ} = 3.8 \text{ kcal mol}^{-1}$ ($= 2.3RT\Delta\text{p}K_{\text{a}}$). Whereas for toluene C–H⁴⁸ and $[\text{HPd}(\text{diphosphine})_2]^+ \text{Pd-H}$ ^{49a} bond strengths, $F\Delta E_{1/2}$ and $2.3RT\Delta\text{p}K_{\text{a}}$ are equal in magnitude; for the acac versus

- (45) Examples of isolated hydrogen atom abstractors (X^{\bullet}) with relative high X–H BDEs (ignoring entropy differences between X and HX , $\text{BDFE}(\text{X-H}) \cong \text{BDE}(\text{X-H}) - 5 \text{ kcal mol}^{-1}$ in organic solvents^{7b}): (a) $[\text{Fe}^{\text{II}}(\text{PY5})(\text{OMe})]^{2+}$ ($\text{PY5} = 2,6\text{-bis}(\text{bis}(2\text{-pyridyl})\text{methoxymethane})\text{-pyridine}$), BDE = $83.5 \text{ kcal mol}^{-1}$ in MeOH: Goldsmith, C. R.; Jonas, R. T.; Stack, T. D. P. *J. Am. Chem. Soc.* **2002**, *124*, 83. (b) $[\text{Mn}^{\text{III}}(\text{PY5})(\text{OH})]^{2+}$, BDE = 82 kcal mol^{-1} in MeCN: Goldsmith, C. R.; Cole, A. P.; Stack, T. D. P. *J. Am. Chem. Soc.* **2005**, *127*, 9904. (c) $[\text{Mn}^{\text{III}}(\text{H}_3\text{I})\text{O}]^{2-}$ ($\text{H}_3\text{I} = \text{tris}[(N\text{-tert-butylureaylato})\text{-}N\text{-ethyl}]\text{aminato}$), BDE = 77 kcal mol^{-1} in DMSO ($[\text{Mn}^{\text{IV}}(\text{H}_3\text{I})\text{O}]^{2-}$ and $[\text{Fe}^{\text{IV}}(\text{H}_3\text{I})\text{O}]^{2-}$, BDEs = 110 and $115 \text{ kcal mol}^{-1}$, were not isolated.): Gupta, R.; Borovik, A. S. *J. Am. Chem. Soc.* **2003**, *125*, 13234. (d) $[\text{Ru}^{\text{IV}}(\text{bpy})_2(\text{py})\text{O}]^{2+}$, BDE = 84 kcal mol^{-1} in MeCN: ref. 1e and Bryant, J. R.; Mayer, J. M. *J. Am. Chem. Soc.* **2003**, *125*, 10351. (e) $\text{Mn}^{\text{VII}}\text{O}_4^-$, BDE = 80 kcal mol^{-1} in H_2O ; $[\text{Mn}_2(\mu\text{-O})_2(\text{phen})_4]^{3+}$ ($\text{phen} = 1,10\text{-phenanthroline}$), BDE = 79 kcal mol^{-1} in MeCN: ref. 3. (f) $[\text{Tp}^{\text{Bu.Me}}\text{Cr}^{\text{IV}}(\text{py}/\text{H})]^+$ ($\text{Tp}^{\text{Bu.Me}} = \text{hydrotris}(3\text{-tert-butyl-5-methylpyrazolyl})\text{-borate}$, $\text{py}/\text{H} = 3\text{-tert-butyl-5-methylpyrazole}$), BDE > $75.3 \text{ kcal mol}^{-1}$ in CD_2Cl_2 : Qin, K.; Incarvito, C. D.; Rheingold, A. L.; Theopold, K. H. *J. Am. Chem. Soc.* **2002**, *124*, 14008. (g) $[\text{Fe}^{\text{IV}}(\text{O})(\text{N4Py})]^{2+}$ and $[\text{Fe}^{\text{IV}}(\text{O})(\text{Bn-tpen})]^{2+}$ ($\text{N4Py} = N,N\text{-bis}(2\text{-pyridylmethyl})\text{-}N\text{-bis}(2\text{-pyridyl})\text{methylamine}$, $\text{Bn-tpen} = N\text{-benzyl-}N,N'\text{-tris}(2\text{-pyridylmethyl})\text{ethylenediamine}$) oxidize C–H bonds of cyclohexane (BDE $\approx 99.3 \text{ kcal mol}^{-1}$) in MeCN: Kaizer, J.; Klinker, E. J.; Oh, N. Y.; Rohde, J.-U.; Song, W. J.; Stubna, A.; Kim, J.; Münck, E.; Nam, W.; Que, L., Jr. (h) *tri-tert-butylphenoxyl radical*, BDE = $82.3 \text{ kcal mol}^{-1}$ in DMSO: Bordwell, F. G.; Liu, W. Z. *J. Am. Chem. Soc.* **1996**, *118*, 10819.
- (46) The $\Delta E_{1/2}$ (0.99 V) reported here is calculated from $E_{1/2}$ values of *cis*- $[\text{Ru}(\text{acac})_2(\text{MeCN})_2]^{+/0}$ and *cis*- $[\text{Ru}(\text{hfac})_2(\text{MeCN})_2]^{+/0}$ (-0.29 and 0.70 V vs $\text{Cp}_2\text{Fe}^{+/0}$) measured in this work, which agree very well with those predicted by Lever parameters (-0.28 and 0.69 V)⁴⁷ but differ significantly from those reported in ref 15 ($\Delta E_{1/2} = 1.22 \text{ V}$).
- (47) Lever, A. B. P. *Inorg. Chem.* **1990**, *29*, 1271.
- (48) Pratt, D. A.; DiLabio, G. A.; Mulder, P.; Ingold, K. U. *Acc. Chem. Res.* **2004**, *37*, 334.
- (49) (a) Raebiger, J. W.; Miedaner, A.; Curtis, C. J.; Miller, S. M.; Anderson, O. P.; DuBois, D. L. *J. Am. Chem. Soc.* **2004**, *126*, 5502. (b) Frazee, K.; Wilson, A. D.; Appel, A. M.; Rakowski, DuBois, M.; DuBois, D. L. *Organometallics* **2007**, *26*, 3918–3924.

(43) Gas-phase thermochemical data from NIST Chemistry Webbook, June 2005 release.

(44) This analysis follows that in Soper, J. D.; Rhile, I. J.; DiPasquale, A. G.; Mayer, J. M. *Polyhedron* **2004**, *23*, 323 and references therein.

hfac complexes, $F\Delta E_{1/2}$ is 5.6 times as large as $2.3RT\Delta pK_a$. The disconnection between $\Delta E_{1/2}$ and ΔpK_a is likely due to the four CF_3/CH_3 groups being six bonds removed from the N–H bond, causing little effect on the loss of the proton, but only three bonds removed from the ruthenium center that at least formally loses the electron.

Conclusions

A ruthenium acac pyridine–imidazole system has been developed that is very well suited for the study of metal-mediated hydrogen atom transfer. Both the Ru^{II} protonated and Ru^{III} deprotonated complexes, Ru^{II}(acac)₂(py-imH) (**1**) and Ru^{III}(acac)₂(py-im) (**3**), have been isolated and well characterized, fulfilling our design criteria of suitable one-electron reduction potential couples between protonated and mono-deprotonated species for the Ru^{II} and Ru^{III} states. The reduction potential and pK_a measurements indicate that the removal of a H[•] from the imidazole N–H in **1** has a BDFE of 62.0 kcal mol⁻¹ in MeCN at 298 K, and 79.6 kcal mol⁻¹ in Ru^{II}(hfac)₂(py-imH) (**4**). The remarkable 17.6 kcal mol⁻¹ difference in BDFEs is primarily due to an increase in $E_{1/2}$ (0.93 V, 21.4 kcal mol⁻¹) with small compensation from the decrease of pK_a (2.8 units, 3.8 kcal mol⁻¹), when substituting two acac for hfac ligands. Consistent with the BDFEs in **1** and **4**, complex **1** is very rapidly oxidized by TEMPO[•] to give **3** and TEMPO–H in a net HAT reaction, for which $\Delta G^\circ = -4.5$ kcal mol⁻¹. In contrast, no reaction was observed between **4** and TEMPO[•], consistent with a very uphill $\Delta G^\circ = +13.1$ kcal mol⁻¹, and a facile reaction occurs in the opposite direction: Ru^{III}(hfac)₂(py-im) (**6**) + TEMPO–H \rightarrow **4** + TEMPO[•]. Detailed studies of HAT reactions with these systems are underway, including HAT self-exchange, kinetic isotope effects, and application of the Marcus cross relation.

Experimental Section

Materials. All of the reagent grade solvents were purchased from Fisher Scientific, EMD Chemicals, or Honeywell Burdick & Jackson (for anhydrous MeCN). Various efforts to purify MeCN, including treatments with CaH₂/P₂O₅ and various oxidants, have only decreased the stability of strongly oxidizing materials in MeCN (perhaps due to amine impurities). Therefore, the high-purity Burdick & Jackson MeCN was simply sparged with N₂ and piped from a steel keg directly into a glove box. Deuterated solvents were obtained from Cambridge Isotope Laboratories. CD₃CN was dried over CaH₂, vacuum transferred to P₂O₅, then over to CaH₂, and then to an empty glass vessel. DBU, 2,4-lutidine, TEMPO[•], and (ⁿBu₄N)PF₆ were purchased from Aldrich, HOTf from Acros, and Et₃N from Fisher. Et₃N was distilled from KOH and then dried over CaH₂.⁵⁰ TEMPO[•] was sublimed onto a cold finger. (ⁿBu₄N)-PF₆ was recrystallized from EtOH before use. *cis*-Ru^{II}(acac)₂(MeCN)₂,¹⁴ *cis*-[Ru^{III}(acac)₂(MeCN)₂]OTf,¹⁵ *cis*-Ru^{II}(hfac)₂(MeCN)₂,¹⁵ py-imH,¹² py-imnH,³⁵ TEMPO–H,³² and [N(tol)₃]PF₆³³ were prepared according to literature procedures. All of the reactions were performed in the absence of air, using glove box/vacuum line techniques unless otherwise noted.

Physical Techniques and Instrumentation. ¹H (300 and 500 MHz), ¹³C{¹H} (75 and 126 MHz), and ¹⁹F (282 MHz) NMR and ¹H 2D COSY spectra were recorded on Bruker Avance spectrometers at room temperature, referenced to a residual solvent peak or an external CF₃C(O)OH standard ($\delta = -78.50$),²⁴ and reported as: δ (multiplicity, number of protons, assignment, coupling constant). The error for NMR integration is estimated to be $\pm 10\%$. Electron impact mass spectra (EI/MS) were obtained on a Kratos Profile HV-3 direct probe instrument. Electrospray ionization mass spectra (ESI/MS) were obtained on a Bruker Esquire-LC ion trap mass spectrometer and reported as m/z for the most-abundant peak in a ruthenium isotopic pattern. Samples were infused as MeCN solutions and acquired in positive- or negative-ionization mode. UV–vis spectra were acquired with a Hewlett-Packard 8453 diode array spectrophotometer in anhydrous MeCN, and are reported as λ_{\max}/nm ($\epsilon/M^{-1} \text{ cm}^{-1}$). CV measurements in 0.1 M (ⁿBu₄N)PF₆/MeCN were performed using a platinum disc working electrode, a platinum wire auxiliary electrode, and a silver wire/AgNO₃ reference electrode with Cp₂Fe as an internal standard, and potentials are reported versus Cp₂Fe⁺⁰ (± 0.01 V). Elemental analyses were performed by Atlantic Microlab (Norcross, GA).

Ru^{II}(acac)₂(py-imH) (1). A solution of *cis*-Ru^{II}(acac)₂(MeCN)₂ (150 mg, 0.393 mmol) and py-imH (69 mg, 0.48 mmol) in C₆H₆ (15 mL) was stirred and heated in a 80 °C oil bath for 5 h under N₂. The solution was cooled to room temperature to yield a brown precipitate, which was filtered by a swivel frit and dried in vacuo. Yield: 136 mg (78%). ¹H NMR (CD₃CN): 1.51 (6H), 2.00 (3H), 2.05 (3H) (s, acac–CH₃); 5.29, 5.32 (s, 1H each, acac–CH); 7.09 (t), 7.53 (t), 7.81 (d), 8.75 (d) (1H each, py-H, ³J_{HH} = 6–8 Hz); 7.14, 7.36 (d, 1H each, im–CH, ³J_{HH} = 2 Hz); 11.31 (s, 1H, im–NH). An adequate ¹³C{¹H} NMR spectrum has not been obtained due to low solubility of **1**. EI/MS: 444 [M – H]⁺, 401, 344 [M – acacH]⁺, 300 [M – py-imH]⁺, 259, 247. UV–vis: 272 (27 000), 428 (6700), 568 (7000). CV: $E_{1/2} = -0.64$ V (Ru^{III/II}). Anal. Calcd (Found) for C₁₈H₂₁N₃O₄Ru: C, 48.64 (48.84); H, 4.76 (4.71); N, 9.45 (9.18).

[Ru^{III}(acac)₂(py-imH)]OTf (2). A solution of *cis*-[Ru^{III}(acac)₂(MeCN)₂]OTf (150 mg, 0.283 mmol) and py-imH (49 mg, 0.34 mmol) in C₆H₆ (15 mL) was stirred under N₂ at 80 °C for 5 h. The solution was cooled to room temperature to yield a brick-red precipitate, which was filtered by a swivel frit. The solid was reprecipitated with CH₂Cl₂/hexanes, filtered, and dried in vacuo at 78 °C. Yield: 125 mg (74%). ¹H NMR (CD₃CN): (all br s) –21.71 (6H), –18.88 (3H), –17.48 (3H) (acac–CH₃); –64.83, –54.40, –23.61, –8.07 (1H each, acac–CH or im–CH); –8.87, 0.07, 2.14, 3.91 (1H each, py-H); 5.71 (1H, im–NH). EI/MS: 444 [M–H]⁺, 401, 344 [M – acacH]⁺, 300 [M – py-imH]⁺, 259, 247. ESI/MS⁺: 445 (M⁺); ESI/MS⁻: 149 (OTf⁻). UV–vis: 288 (20 000), 360sh (5000), 520 (2000). CV: $E_{1/2} = -0.64$ V (Ru^{III/II}). Anal. Calcd (Found) for C₁₉H₂₁N₃O₇F₃SRu: C, 38.45 (38.27); H, 3.57 (3.59); N, 7.08 (7.31).

Ru^{III}(acac)₂(py-im) (3). A solution of **1** (200 mg, 0.450 mmol) and TEMPO[•] (84 mg, 0.54 mmol) in MeCN (30 mL) was stirred under N₂ for 10 min at room temperature. The solvent was removed under vacuum, and the residue was sublimed for 16 h with a vacuum cold finger apparatus to remove TEMPO–H. The product was reprecipitated with CH₂Cl₂/hexanes to yield a dark-brown solid, which was filtered and dried in vacuo at 78 °C. Yield: 130 mg (65%). ¹H NMR (CD₃CN): (all br s) –17.58, –15.52, –11.00, –5.09 (3H each, acac–CH₃); –47.33, –39.08, –21.31, –19.45 (1H each, acac–CH or im–CH); –8.56, –4.46, –2.95, 8.75 (1H each, py-H). EI/MS: 444 (M⁺), 401, 344 [M – acac]⁺, 300 [M – py-im]⁺, 259, 247. ESI/MS⁺: 445 [M + H]⁺. UV–vis: 286

(50) Armarego, W. L. F.; Chai, C. L. L. *Purification of Laboratory Chemicals 5th Ed.*; Butterworth-Heinemann: Amsterdam, The Netherlands, 2003.

(19 000), 331sh (13 000), 486 (1600). CV: $E_{1/2} = -1.00$ V (Ru^{III/II}). Anal. Calcd (Found) for C₁₈H₂₀N₃O₄Ru·0.2H₂O: C, 48.36 (47.89); H, 4.60 (4.51); N, 9.40 (9.35); ¹H NMR spectra of **3** in CD₃CN typically show ~0.2 equiv of H₂O per ruthenium although an NMR spectrum of the batch sent for elemental analysis was not obtained.

Ru^{II}(hfac)₂(py-imH) (4). A solution of *cis*-Ru^{II}(hfac)₂(MeCN)₂ (1000 mg, 1.67 mmol) and py-imH (420 mg, 2.89 mmol) in C₆H₆ (50 mL) was refluxed for 16 h under air. The solvent was removed on a rotary evaporator, and the residue was loaded onto a silica gel column and eluted with 9:1 CH₂Cl₂/CH₃OH. The first brown fraction was unreacted *cis*-Ru^{II}(hfac)₂(MeCN)₂ (207 mg, 21%), and **4** was isolated as the second red-brown fraction, which was rotary evaporated to dryness, reprecipitated with CH₂Cl₂/hexanes, filtered, and dried in vacuo at 78 °C. Yield: 298 mg (27%). ¹H NMR (CD₃-CN): 6.20 (s, 2H, hfac-H); 7.42 (t), 7.97 (t), 8.09 (d), 8.48 (d) (1H each, py-H, ³J_{HH} = 6–8 Hz); 7.22, 7.49 (d, 1H each, im-CH, ³J_{HH} = 2 Hz); 11.82 (s, 1H, im-NH). ¹⁹F NMR (CD₃CN): -75.06, -75.04, -74.99, -74.94 (s, hfac-CF₃). ¹³C{¹H} NMR (CD₃OD): 92.81, 93.00 (hfac-CH); 117.84, 117.86, 119.02, 119.09 (q, hfac-CF₃, ¹J_{CF} = 282 Hz); 120.83, 124.81, 137.99, 153.41 (py-CH); 121.53, 132.38 (im-CH); 149.67, 153.26 (py-N-C-C-N-im); 168.94, 169.10, 172.35, 172.53 (q, hfac-C(O), ²J_{CF} = 33 Hz). ESI/MS⁺: 661 (M⁺). UV-vis: 291 (26 000), 481sh (9600), 519 (10 000). CV: $E_{1/2} = 0.29$ V (Ru^{III/II}). Anal. Calcd (Found) for C₁₈H₉F₁₂N₃O₄Ru: C, 32.74 (32.80); H, 1.37 (1.38); N, 6.36 (6.54).

[DBU-H][Ru^{II}(hfac)₂(py-im)] (5). DBU (25 μL, 0.165 mmol) was added to a red-brown solution of **4** (109 mg, 0.165 mmol) in MeCN (10 mL) under air to immediately generate a dark-purple solution, which was rotary evaporated to dryness. The residue was reprecipitated with CH₂Cl₂/hexanes to yield a black-purple solid, which was filtered and dried in vacuo at 78 °C. Yield: 102 mg (76%). ¹H NMR (CD₃CN): 1.70 (m, 6H), 1.98 (quintet, 2H), 2.60 (m, 2H), 3.30 (t, 2H), 3.46 (t, 2H), 3.52 (m, 2H) (DBU-H⁺); 6.11, 6.12 (s, 1H each, hfac-H); 7.06 (t), 7.71 (t), 7.87 (d), 8.21 (d) (1H each, py-H, ³J_{HH} = 6–8 Hz); 6.99, 7.19 (d, 1H each, im-CH, ³J_{HH} = 2 Hz). ¹⁹F NMR (CD₃CN): -75.06, -74.91, -74.88, -74.74 (s, hfac-CF₃). ¹³C{¹H} NMR (CD₃OD): 20.43, 24.94, 27.49, 29.96, 33.78, 39.42, 49 (overlapped with CD₃OD), 55.36 (DBU-CH₂); 93.38, 93.47 (hfac-CH); 118.23, 119.74, 119.58 (q, hfac-CF₃, ¹J_{CF} = 282 Hz), the fourth quartet is obscured by overlapping with py-CH; 118.56, 121.18, 137.01, 152.09 (py-CH); 129.80, 132.11 (im-CH); 155.76, 167.45 (py-N-C-C-N-im); 158.29 (DBU-N=C-N); 165.70, 166.68, 170.13, 170.83 (q, hfac-C(O), ²J_{CF} = 33 Hz). ESI/MS⁺: 661 [M + H]⁺, 153 (DBU-H⁺); ESI/MS⁻: 660 (M⁻). UV-vis: 292 (20 000), 472 (8300), 564 (11 000). CV: $E_{1/2} = -0.07$ V (Ru^{III/II}). Anal. Calcd (Found) for C₂₇H₂₅F₁₂N₅O₄Ru: C, 39.91 (39.92); H, 3.10 (3.11); N, 8.62 (8.74).

In Situ Generation of Ru^{III}(hfac)₂(py-im) (6) and Reaction of 6 + TEMPO-H. In a N₂ glove box, solutions of **5** (2.5 mM, 4.0 mg in 2.0 mL), [N(tol)₃]PF₆ (61.5 mM, 26.6 mg in 1 mL), and TEMPO-H (123 mM, 38.7 mg in 2.0 mL) in CD₃CN were prepared at room temperature. A trace amount of (Me₃Si)₂O was added to the solution of **5** as internal standard. Each of three J-Young NMR tubes were filled with 0.5 mL of the solution of **5**. To tubes 2 and 3 was added 1 equiv of [N(tol)₃]PF₆ (20 μL), with immediate color changes from purple-red to pale-brown **6**. After mixing tube 3 well, 1 equiv of TEMPO-H (10 μL) was added, giving an immediate color change to red-brown **4**. The ¹H NMR spectrum of tube 2 after ~20 min showed resonances of DBU-H⁺, N(tol)₃ [δ 2.27 (s, 9H, CH₃); 6.87, 7.07 (d, 6H each, Ar-H, ³J_{HH} = 7 Hz)], and a trace of **4**; paramagnetic **6** was not observed. The ¹H NMR spectrum of tube 3 showed 100 ± 10% yield for **4**, on the basis of the integration of starting **5**. The generation of **6** was also monitored

by UV-vis titration (Figure S4 in the Supporting Information). Inside a glove box, solutions of **5** (0.053 mM), [N(tol)₃]PF₆ (2.7 mM), and TEMPO-H (2.7 mM) in MeCN were prepared at room temperature. An aliquot of **5** (2.5 mL) in a UV-vis cuvette was titrated with 0.1 equiv (5 μL) increments of [N(tol)₃]PF₆ until 1 equiv, as **6** was generated. UV-vis of **6**: 455 (4700), 508 (3400). The solution was further titrated with increments of 0.1 equiv (5 μL) of TEMPO-H until 1 equiv, as **4** was produced. The yield for **4** was 100 ± 10% on the basis of starting **5**. CV: $E_{1/2} = -0.07$ V (Ru^{III/II}) for **6**, generated from **5** (2.5 mM, 2.0 mL) + 1 equiv of [N(tol)₃]PF₆ (62 mM, 80 μL) in MeCN.

Ru^{II}(acac)₂(py-imnH) (7). Complex **7** was synthesized analogous to **1** using *cis*-Ru^{II}(acac)₂(MeCN)₂ (200 mg, 0.52 mmol) and py-imnH (93 mg, 0.63 mmol) and was isolated as a black-green powder. Yield: 121 mg (52%). ¹H NMR (CD₃CN): 1.55 (3H), 1.60 (3H), 2.00 (6H) (s, acac-CH₃); 3.6–4.0 (m, 4H, imn-CH), 5.27, 5.31 (1H each, acac-CH); 6.12 (s, 1H, imn-NH); 7.12 (t), 7.49 (t), 7.61 (d), 8.74 (d) (1H each, py-H, ³J_{HH} = 6–8 Hz). An adequate ¹³C{¹H} NMR spectrum has not been obtained because of low solubility of **7**. EI/MS: 447 [M]⁺, 348 [M - acac]⁺, 300 [M - py-imnH]⁺, 282, 276, 260, 248. UV-vis: 274 (24 000), 428 (6900), 610 (7700). CV: $E_{1/2} = -0.68$ V (Ru^{III/II}). Anal. Calcd (found) for C₁₈H₂₃N₃O₄Ru: C, 48.42 (48.13); H, 5.19 (5.26); N, 9.41 (9.38).

Ru^{II}(hfac)₂(py-imnH) (8). Complex **8** was synthesized analogous to **4** except using *cis*-Ru^{II}(hfac)₂(MeCN)₂ (200 mg, 0.33 mmol) and py-imnH (99 mg, 0.67 mmol) and was isolated as a brown-purple powder. Yield: 62 mg (28%). ¹H NMR (CD₃CN): 3.72 (1H), 3.85 (1H), 4.00 (2H) (m, imn-CH); 6.17, 6.20 (s, 1H each, hfac-H); 6.90 (s, 1H, imn-NH); 7.50 (t), 7.95 (t), 7.97 (d), 8.54 (d) (1H each, py-H, ³J_{HH} = 6–8 Hz). ¹⁹F NMR (CD₃CN): -75.14, -75.11, -75.01, -74.83 (s, hfac-CF₃). ¹³C{¹H} NMR (CD₃OD): 46.12, 55.58 (imn-CH); 92.86 (both hfac-CH); 117.89, 117.96, 119.04, 119.12 (q, hfac-CF₃, ¹J_{CF} = 282 Hz); 125.02, 127.16, 137.45, 153.84 (py-CH); 152.92, 169.34 (py-N-C-C-N-imn); 168.22, 169.59, 172.25, 172.50 (q, hfac-C(O), ²J_{CF} = 33 Hz). ESI/MS⁺: 663 (M⁺). UV-vis: 225 (6200), 269 (5300), 289 (5300), 484sh (4200), 524 (5300). CV: $E_{1/2} = 0.14$ V (Ru^{III/II}). Anal. Calcd (Found) for C₁₈H₁₁F₁₂N₃O₄Ru: C, 32.64 (32.82); H, 1.67 (1.67); N, 6.34 (6.30).

¹H NMR Titration of 2 and 3. Stock solutions were prepared for DBU (111 mM, 16.9 mg in 1 mL) and HOTf (111 mM, 16.7 mg in 1 mL) in CD₃CN. A solution of **3** in an NMR tube (11 mM, 2.5 mg in 0.5 mL CD₃CN) was titrated to **2** by adding 1 equiv of HOTf in 0.1 equiv (5 μL) increments. ¹H NMR spectra were recorded initially and after each addition of HOTf. Each peak in the spectra was a weighted average of the corresponding peaks for **2** and **3**, indicating fast proton exchange on the NMR time scale. The reverse titration, adding 1 equiv of DBU in 0.1 equiv (5 μL) increments, was also monitored by ¹H NMR.

UV-Vis Titration of 2 and pK_a Determination. Stock solutions were prepared for **2** (0.11 mM), DBU (6.5 mM), and HOTf (6.5 mM) in MeCN. An aliquot of **2** (3.0 mL, 0.11 mM) was transferred to a UV-vis cuvette and was titrated with increments of 0.1 equiv (5 μL) of DBU. UV-vis spectra were recorded for the initial **2** and after each addition of DBU. A total of 1.3 equiv of DBU was added, but the spectrum stopped changing after 1.0 equiv, showing a stoichiometric conversion to the deprotonated **3**. The titration was reversible, and protonated **2** was regenerated stoichiometrically by 1 equiv of HOTf, by adding 0.1 equiv (5 μL) increments.

A stock solution of 2,4-lutidine (647 mM) in MeCN was prepared, and was serially diluted twice to make two other solutions (64.7 and 6.47 mM). An aliquot of **2** (3.0 mL, 0.11 mM) was

transferred to a UV-vis cuvette and was titrated with increments of 0.1 equiv (5 μ L) of 2,4-lutidine (6.47 mM) until 2.0 equiv. The titration was continued by adding 1 equiv (5 μ L) of 64.7 mM base until 20 equiv and then with 10 equiv (5 μ L) of 647 mM base until 200 equiv. UV-vis spectra were recorded for the initial **2** and after each addition of 2,4-lutidine. The UV-vis data were analyzed using the absorbance at 340 nm, yielding $[3]/[2] = (A - A_2)/(A_3 - A)$, where A_2 and A_3 are the absorbances for pure **2** and **3** at 340 nm: $[3] = [2,4\text{-lutidine-H}^+] = \{((A - A_2)/(A_3 - A_2)) \times [\text{Ru}]_{\text{total}}\}$ and $[2,4\text{-lutidine}] = [2,4\text{-lutidine}]_{\text{total}} - [2,4\text{-lutidine-H}^+] = [2,4\text{-lutidine}]_{\text{total}} - \{((A - A_2)/(A_3 - A_2)) \times [\text{Ru}]_{\text{total}}\}$. Plotting $[3]/[2,4\text{-lutidine-H}^+]/[2]$ versus $[2,4\text{-lutidine}]$ yielded a straight line (Figure S3 in the Supporting Information), whose slope is $K_{\text{eq}} = 0.011 \pm 0.001$ for $\mathbf{2} + 2,4\text{-lutidine} \rightleftharpoons \mathbf{3} + (2,4\text{-lutidine-H})\text{OTf}$. The $\text{p}K_{\text{a}}$ of **2** was calculated from $\text{p}K_{\text{a}}(\mathbf{2}) = \text{p}K_{\text{a}}(2,4\text{-lutidine-H}^+) - \log K_{\text{eq}} = 16.0 \pm 0.1$ using the known $\text{p}K_{\text{a}}$ of 14.05 for 2,4-lutidine-H⁺.²⁷

UV-Vis Titration of 4 and $\text{p}K_{\text{a}}$ Determination. Following the procedure above, 3.0 mL of a 0.033 mM solution of **4** was titrated with DBU (19.6 mM) and then with HOTf (19.7 mM) (all in MeCN). One equiv of DBU completely converted **4** to **5**, which was converted back to **4** by 1 equiv of HOTf. Again, following the procedure above, **4** (3.0 mL, 0.030 mM) was titrated with solutions of Et₃N, adding 0.1 equiv (5 μ L) of Et₃N (1.78 mM) until 2.0 equiv, then adding 1 equiv (5 μ L) of Et₃N (17.8 mM) until 20 equiv. UV-vis spectra were recorded for the initial **4** and after each addition of Et₃N, and the data were analyzed using the absorbance at 565 nm. The plot of $[5][\text{Et}_3\text{NH}^+]/[4]$ versus $[\text{Et}_3\text{N}]$ yielded a straight line with slope $K_{\text{eq}} = 0.14 \pm 0.01$. The $\text{p}K_{\text{a}}$ of **4** is given by $\text{p}K_{\text{a}}(\mathbf{4}) = \text{p}K_{\text{a}}(\text{Et}_3\text{NH}^+) - \log K_{\text{eq}} = 19.3 \pm 0.1$ using $\text{p}K_{\text{a}} = 18.46$ for Et₃NH⁺.²⁷

¹H NMR Reactions with TEMPO[•]. Many reactions were monitored by ¹H NMR in sealable J-Young tubes. In a typical procedure, solutions of **1** (1.8 mM, 1.6 mg in 2 mL) and TEMPO[•] (90 mM, 28.0 mg in 2 mL) were prepared in CD₃CN in a N₂ glove box. A trace of (Me₃Si)₂O was added to the solution of **1** as an internal standard. Each of the two J-Young tubes was charged with 0.5 mL of the solution of **1**. TEMPO[•] (1 equiv, 10 μ L) was added to one of the tubes, accompanied by an instant color change from red-purple to pale-brown. ¹H NMR spectra of **1** and **1** + TEMPO[•] were recorded after ~20 min, the latter showing the product yield for **3** (86%) and TEMPO-H (98%) [TEMPO-H: δ 1.06 (s, 12H, CH₃), 1.45 (s, 6H, CH₂), 5.34 (s, 1H, OH)].³² The ¹H NMR spectrum of **4** (3.0 mM, 0.5 mL) and 36 equiv of TEMPO[•] (8.5 mg) in CD₃CN showed resonances only for **4** and TEMPO[•] at room temperature after 1 d [TEMPO[•]: δ -29.74 (4H, 3,5-CH₂), -16.51 (12H, CH₃), 15.33 (2H, 4-CH₂) (all br s)].

X-ray Structural Determinations. Crystals of **1** were grown from the slow evaporation of MeCN/C₆H₆ solutions inside a N₂ glove box. Crystals of **2–5** and **8** were grown by vapor diffusion of Et₂O/hexanes to CH₂Cl₂ solutions of the complex under air. The crystals were mounted onto glass capillaries with oil. The data were collected on a Nonius Kappa CCD diffractometer. The data were integrated and scaled using *hkl-SCALEPACK*.⁵¹ This program applies multiplicative correction factor (*S*) to the observed intensities (*I*) and has the following form: $S = \exp(-2B(\sin^2\theta)/\lambda^2)/\text{scale}$. *S* is calculated from the scale, and *B* factor determined for each frame and is then applied to *I* to give the corrected intensity (*I*_{corr}). Solution by direct methods (*SIR97*) produced a complete heavy-atom phasing model consistent with the proposed structure.⁵² All of the hydrogen atoms were located using a riding model. All of the non-hydrogen atoms were refined anisotropically by full-matrix least-squares (*SHELXL-97*).⁵³ Half of a solvent molecule per Ru is found in the unit cells of **1** (0.5 C₆H₆) and **2** (0.5 CH₂Cl₂). In the structures of **4** and **8**, each of the unit cells contains two independent ruthenium complexes. The structure of **5** contains a disordered CF₃ group, with major F1, F2, and F3 and minor F1A, F2A, and F3A components (Figure S5 in the Supporting Information); only the major fluorine atoms are shown in part b of Figure 2. The major to minor occupancy was modeled as 80 and 20%, and the thermal ellipsoids for minor components F1A, F2A, and F3A were restrained during refinement.

Acknowledgment. We would like to thank the U.S. National Institutes of Health (GM50422) for financial support of this work. J.M. also thanks Ithaca College Dana Internship Program for a summer fellowship. We acknowledge Mr. Eric Carter and Dr. Mira Kanzelberger for preliminary studies of benzimidazole systems, Ms. Elizabeth Mader for valuable discussions, and Mr. Loren Kruse for assistance with mass spectrometry.

Supporting Information Available: Crystallographic data for **1–5** and **8** in CIF format and Figures S1–S5. This material is available free of charge via the Internet at <http://pubs.acs.org>.

IC7015726

- (51) Otwinowski, Z.; Minor, W. In *Methods in Enzymology*; Carter, C. W., Jr., Sweet, R. M., Eds.; Academic Press: New York, 1997; Vol. 276, pp 307–326.
- (52) Altomare, A.; Casciarano, G.; Giacovazzo, C.; Guagliardi, A.; Burla, M. C.; Polidori, G.; Camalli, M. *J. Appl. Crystallogr.* **1994**, *27*, 435.
- (53) Sheldrick, G. M. *SHELXL-97: Program for the Refinement of Crystal Structures*; University of Göttingen: Göttingen, Germany, 1997.